Cleared for Public Release
Distribution Unlimited

Circuit and Electromagnetic Design Notes

Note 58

July 4, 2009

Switched Oscillators and Their Integration into Helical Antennas

D. V. Giri
Pro-Tech, 11 C Orchard Court, Alamo, CA 94507-1541
Dept. of Electrical and Computer Engg., Univ. of New Mexico, Albuquerque, NM 87131

F. M. Tesche
Holcombe Dept. of Electrical and Computer Engineering
College of Engineering & Science, 337 Fluor Daniel Building
Box 340915, Clemson, SC 29634-0915

M. D. Abdalla and M. C. Skipper
ASR Corporation, 7817 Bursera Dr, NW, Albuquerque, NM 87120

and

Markus Nyffeler
Chief, HPE Laboratory, Spiez, Switzerland

Abstract

In this note, we have addressed the problem of designing, fabricating switched oscillators at four different frequencies, 200MHz, 300MHz, 400MHz and 500 MHz. These oscillators are quarter wavelength long coaxial transmission lines with a nitrogen spark gap switch at one end. We have also fabricated two of these at 200MHz and 500 MHz with a charge voltage of 30 kV. These two oscillators are modeled using PSpice and their output into a 100 Ω load is estimated and tested by fabricating a 100 Ω transmission line. We have then proceeded to use a modified commercial helical antenna with a bandwidth of 400MHz to 600MHz and integrated the switched oscillator into this helical antenna. Measurements have been made of the S_{11}, voltage into the antenna and also transient fields at two distances. *Indeed, starting from electrical power from a 12V battery, electrical field strengths in excess of 10kV/m with damped sinusoidal waveforms at 500 MHz (for example) have been demonstrated.* In summary, 4 switched oscillators are designed, 2 have been fabricated and one of them has been integrated into a helical antenna to form a complete autonomous system.

Contents

1. Introduction

In this note, we report on our investigations into the use of the fundamental MATRIX topology described in references [1, 2, 3, 4 and 5], to generate four separate oscillator modules for operating at center frequencies of 200 MHz, 300 MHz, 400 MHz and 500 MHz. The MATRIX system is designed as an optimized configuration in several regards, and it can be used as a starting point for generating a damped sinusoidal generator for high-power electromagnetic (HPEM) testing.

Baum [1, 2] has described HPEM sources that integrate an oscillator into the antenna system. Examples are: (a) a low–impedance quarter wave transmission-line oscillator feeding a high-impedance antenna, (b) low-impedance half wave transmission-line oscillator feeding a high-impedance antenna. The transmission line oscillator consists of a quarter wave or half wave section of a transmission line (perhaps in oil medium for voltage standoff), that is charged by a high-voltage source. This is schematically shown in Figure 1, where the antenna in this case is a TEM- fed half reflector.

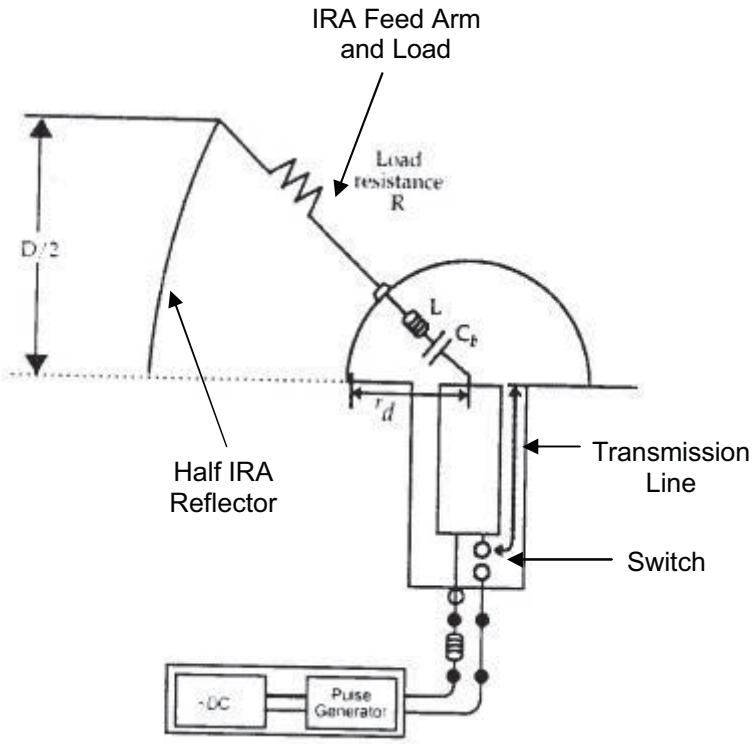

Figure 1. TEM fed reflector.

In this case, there is a switch located across the transmission line as seen in Figure 1, which is self-breaking. When the switch closes a pulsed signal is fed into the antenna connected to this transmission line that radiates an HPEM signal. As an example, 500 MHz corresponds to a quarter wavelength of 15 cm (in SF_6) and 10 cm (in transformer oil) resulting in a very compact source. The charge voltages can be in the range of 100's of kV. The half

wave section doubles the length for a given frequency and thus increases the stored energy. The conceptual design of Figure 1 was implemented and a 180 MHz oscillator called the MATRIX mesoband system [4 and 5] has been built (see Figure 2) and used for testing purposes.

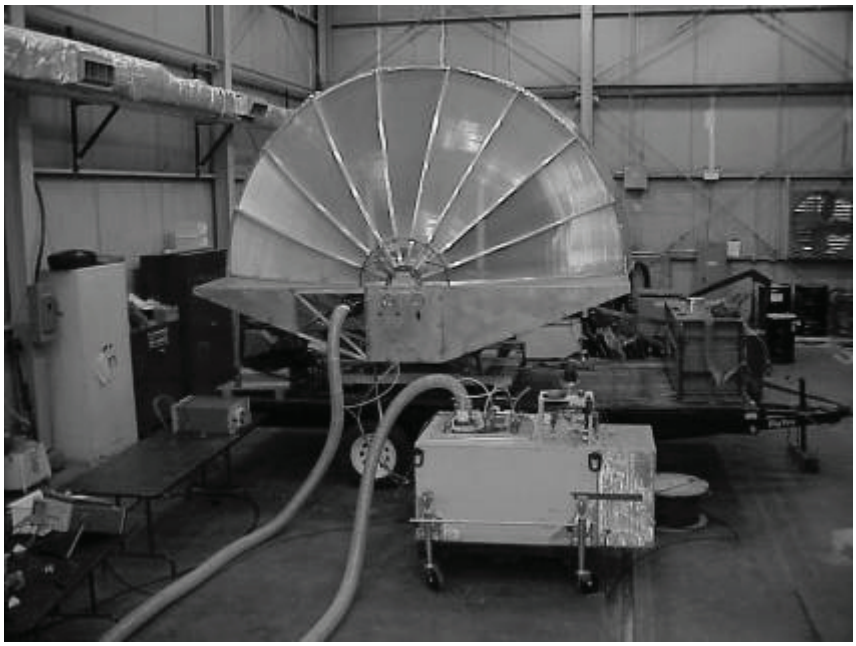

Figure 2. MATRIX (180 MHz oscillator integrated into a TEM fed half reflector)

In these mesoband damped-sinusoidal sources, one of the primary constraints is that the electric fields must be maximum at the switch and must gradually decline from the switch section to the coaxial section. This is to ensure that the switching discharge occurs at the desired switch location, and not at some other high field location in the transmission line.

The ratio of electric fields in the coaxial section to the electric fields in the switch section is a fine balance between minimizing the length of the radial transmission line (RTL) and maximizing the probability that switching events will occur at the switch.

2. Design Goals

The goals of this design study are to:

- Generate preliminary oscillator layouts for four different frequencies.
- Perform PSpice simulations of chosen layouts.

3. Scaling the Existing MATRIX Design

As an example of the design process, let us assume that we want to design the MATRIX for 30 kV charge voltage.

Normally, the MATRIX oscillator would be scaled down by a factor of 10 (30 kV/300 kV) as a starting point for a 30 kV, 200 MHz oscillator. The original switch gap in MATRIX was 2.25 mm for the 300 kV design. However, if we scale it down by a factor of 10, the resulting switch gap would be approximately 0.225 mm, which is quite small and difficult to realize in practice. Given mechanical tolerances of approximately 0.025 mm per part, and that four primary components define the ultimate switch gap; this approach could result in a switch gap variation of as much as 44% [(0.025/0.225) x 4 x 100].

A well defined switch gap is important, not only because it determines the switching voltage/pressure relationship; but also because a change in the gap spacing affects the RTL impedance, which in turn affects the oscillator ring frequency. As a result, mechanical tolerances must be kept as small as is feasible compared to the switch gap dimension.

Consequently, for the 180 MHz MATRIX design, the geometry was scaled down to a minimum switch gap of 0.51 mm and this gives a switch gap potential error of approximately 20%. The resulting scaling factor is 22.67% [(0.51 mm/2.25mm) x 100].

3.1 Electrical Model for the Radial Transmission Line

Scaling the 180 MHz MATRIX oscillator down to a 0.51 mm switching gap yields an RTL section as shown below in Figure 3.

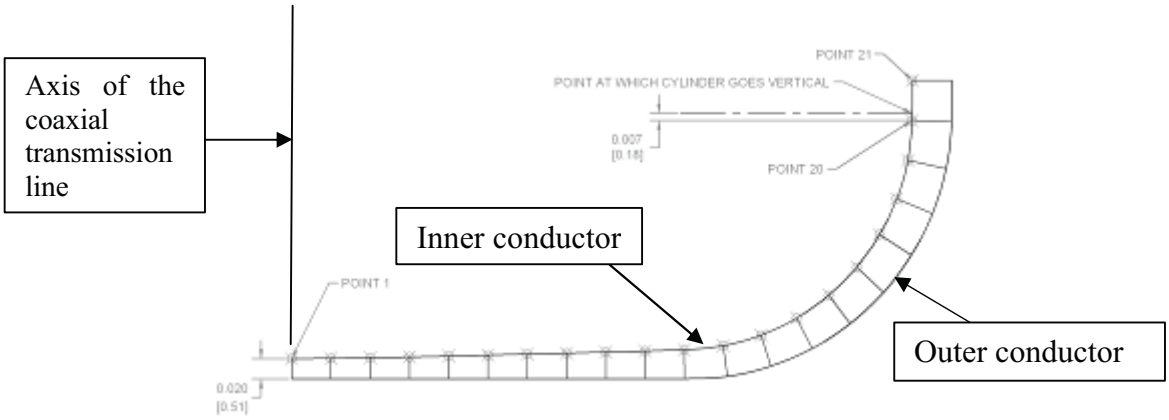

Figure 3. Geometrical arrangement of the radial transmission line (RTL)

To simulate the electrical behavior of the RTL, the radial variation of RTL impedance must be calculated. To do this, the RTL can be divided into 20 equal segments and the coordinates tabulated for each segment. The impedance of each segment can be approximated as

$$Z \approx \frac{377 * d}{2\pi x\sqrt{\varepsilon_r}}, \tag{1}$$

where $2\pi x$ approximates the "width" of each RTL segment, d is the distance between the center conductor and outer conductor (normal to the center conductor) and $\varepsilon_r \sim 1$ for nitrogen and air. Knowing that each RTL segment is 1 mm long, the capacitance of each section is approximated using the following expression:

$$C = \frac{t}{Z_c}. \tag{2}$$

In this equation, t is the segment one way transit time in seconds and Z_c is the characteristic impedance of the RTL segment that was calculated above. The inductance of each segment is then approximated as

$$L = CZ_c^2, \tag{3}$$

where C is the capacitance calculated above.

The overall RTL structure is then simulated in PSpice, with the individual values of L and C representing each segment of the RTL. The spreadsheet used to calculate L and C for each RTL segment can be seen below in Table 1. Each RTL segment was divided into 10 smaller 0.1 mm segment lengths starting from the first segment at the switch location, and progressing radially outward from the switch. The calculated impedance results were then averaged to provide estimates of the impedance of each of the 1 mm segments.

The average impedance over the first 1mm of RTL is calculated as 141 Ω. The variation of RTL impedance versus radial distance from the switch is shown in Figure 4.

Table 1. RTL impedance calculation approach

POINT	X (mm)	Y (mm)	Tline Avg. Radius (mm)	Tline Plate Width (mm)	Plate Sep d (mm)	Z (Ω)	Tline Length (mm)	Tline Length (s)	Tline Capacitance (F)	Tline Inductance (H)
1	0.000	0.000			0.5080	141.4751	1.000	3.333E-12	2.356E-14	4.716E-10
-	0.100	0.000	0.050	0.31416	0.5087	610.4983	0.100	3.333E-13	5.460E-16	2.035E-10
-	0.200	0.001	0.150	0.94248	0.5095	203.7941	0.100	3.333E-13	1.636E-15	6.793E-11
-	0.300	0.001	0.250	1.57080	0.5102	122.4532	0.100	3.333E-13	2.722E-15	4.082E-11
-	0.400	0.002	0.350	2.19911	0.5109	87.59287	0.100	3.333E-13	3.805E-15	2.920E-11
-	0.500	0.002	0.450	2.82743	0.5117	68.22601	0.100	3.333E-13	4.886E-15	2.274E-11
-	0.600	0.003	0.550	3.45575	0.5124	55.90164	0.100	3.333E-13	5.963E-15	1.863E-11
-	0.700	0.004	0.650	4.08407	0.5132	47.36938	0.100	3.333E-13	7.037E-15	1.579E-11
-	0.800	0.005	0.750	4.71239	0.5139	41.11239	0.100	3.333E-13	8.108E-15	1.370E-11
-	0.900	0.006	0.850	5.34071	0.5146	36.32764	0.100	3.333E-13	9.176E-15	1.211E-11
2	0.999	0.007	0.950	5.96742	0.5154	32.55894	1.000	3.333E-12	1.024E-13	1.085E-10
3	1.999	0.024	1.499	9.41997	0.5321	21.29656	1.000	3.333E-12	1.565E-13	7.099E-11
4	2.998	0.042	2.499	15.69995	0.5499	13.20489	1.000	3.333E-12	2.524E-13	4.402E-11
5	3.998	0.063	3.498	21.97914	0.5707	9.789658	1.000	3.333E-12	3.405E-13	3.263E-11
6	4.997	0.088	4.497	28.25752	0.5961	7.953424	1.000	3.333E-12	4.191E-13	2.651E-11
7	5.996	0.114	5.497	34.53591	0.6213	6.782045	1.000	3.333E-12	4.915E-13	2.261E-11
8	6.996	0.139	6.496	40.81509	0.6467	5.973278	1.000	3.333E-12	5.580E-13	1.991E-11
9	7.995	0.164	7.495	47.09427	0.6723	5.382214	1.000	3.333E-12	6.193E-13	1.794E-11
10	8.994	0.189	8.495	53.37266	0.6970	4.923119	1.000	3.333E-12	6.771E-13	1.641E-11
11	9.993	0.218	9.494	59.65024	0.7264	4.591228	1.000	3.333E-12	7.260E-13	1.530E-11
12	10.987	0.319	10.490	65.91107	0.7699	4.403547	1.000	3.333E-12	7.570E-13	1.468E-11
13	11.949	0.584	11.468	72.05540	0.8108	4.242007	1.000	3.333E-12	7.858E-13	1.414E-11
14	12.851	1.011	12.400	77.91086	0.8560	4.14197	1.000	3.333E-12	8.048E-13	1.381E-11
15	13.670	1.581	13.260	83.31627	0.8948	4.049094	1.000	3.333E-12	8.232E-13	1.350E-11
16	14.382	2.279	14.026	88.12800	0.9266	3.963839	1.000	3.333E-12	8.409E-13	1.321E-11
17	14.958	3.094	14.670	92.17687	0.9644	3.944516	1.000	3.333E-12	8.451E-13	1.315E-11
18	15.400	3.989	15.179	95.37192	0.9843	3.890686	1.000	3.333E-12	8.567E-13	1.297E-11
19	15.687	4.944	15.543	97.65969	0.9934	3.834843	1.000	3.333E-12	8.692E-13	1.278E-11
20	15.788	5.938	15.737	98.88137	1.0013	3.817484	1.000	3.333E-12	8.732E-13	1.272E-11
21	15.804	6.937	15.796	99.25163	1.0033	3.810961	1.000	3.333E-12	8.747E-13	1.270E-11

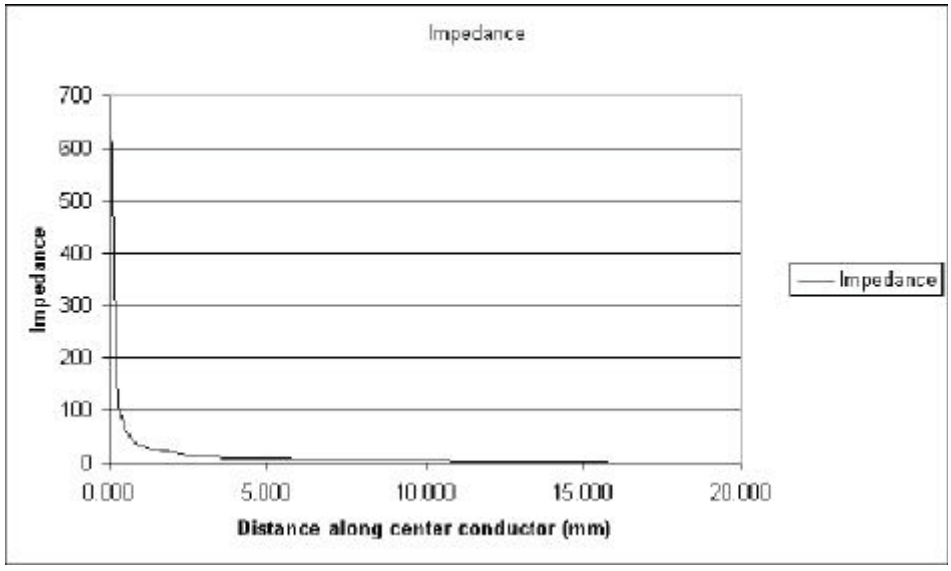

Figure 4. RTL impedance distribution

3.2 The Complete Electrical Model of the RTL

In the PSpice simulation, the RTL lumped element model discussed in the previous section is connected to a uniform 3.7 Ω coaxial transmission line and then to 23 Ω, 66 Ω and 100 Ω load lines to simulate the Ultem insulator, coaxial output and antenna load impedances respectively. The length of the coaxial section is then adjusted to achieve the desired ring frequencies. The PSpice model for the entire oscillator is shown in Figure 5.

The length of coaxial sections to achieve the desired ring frequencies is given in Table 2**Error! Reference source not found.**. The oscillator lengths given in this table assume $\varepsilon_r \sim 1$.

Table 2. Coaxial section lengths required for each frequency

Oscillator Coaxes	T (ns)	L (cm)
200 MHz	0.95	28.5
300 MHz	0.56	16.8
400 MHz	0.36	10.8
500 MHz	0.24	7.2

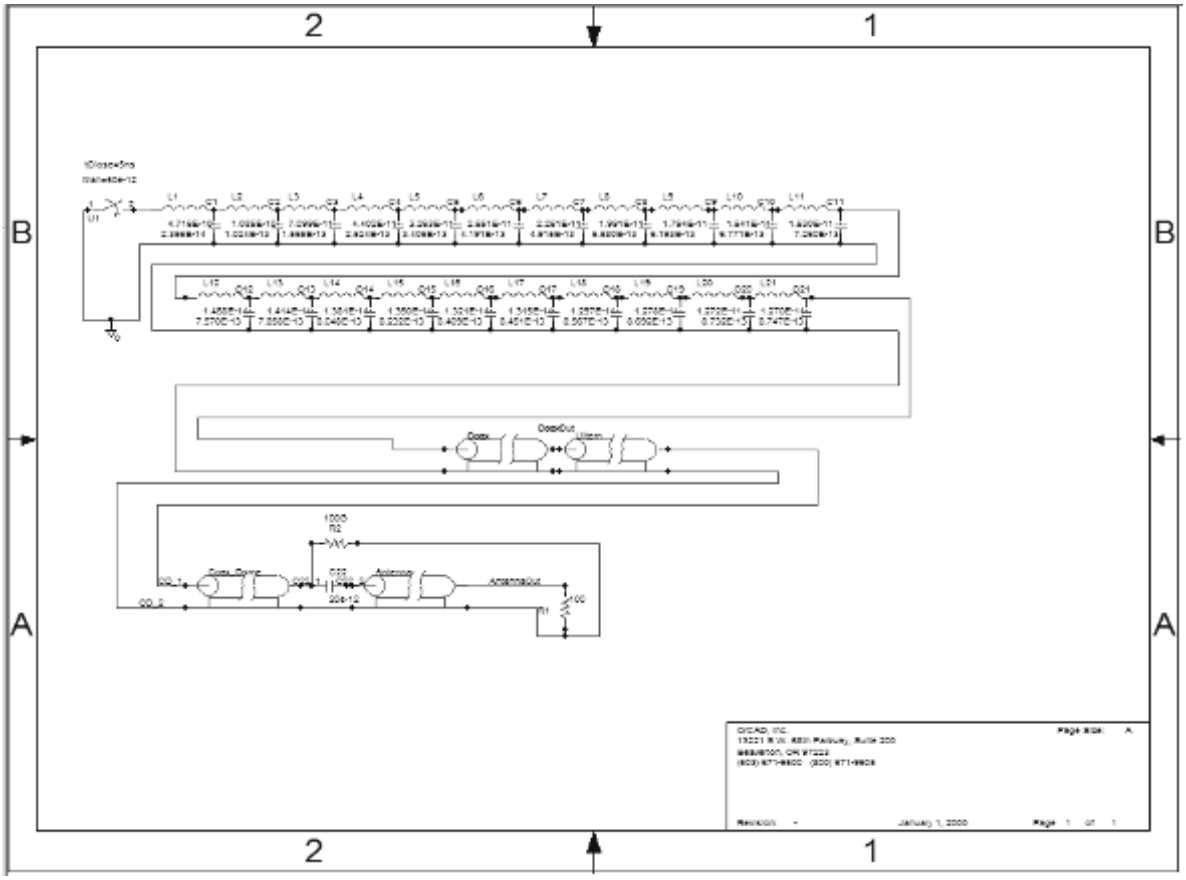

Figure 5. PSpice model for the oscillator

The resulting sizes of the overall oscillator designs are shown in Figure 6, relative to a typical pencil.

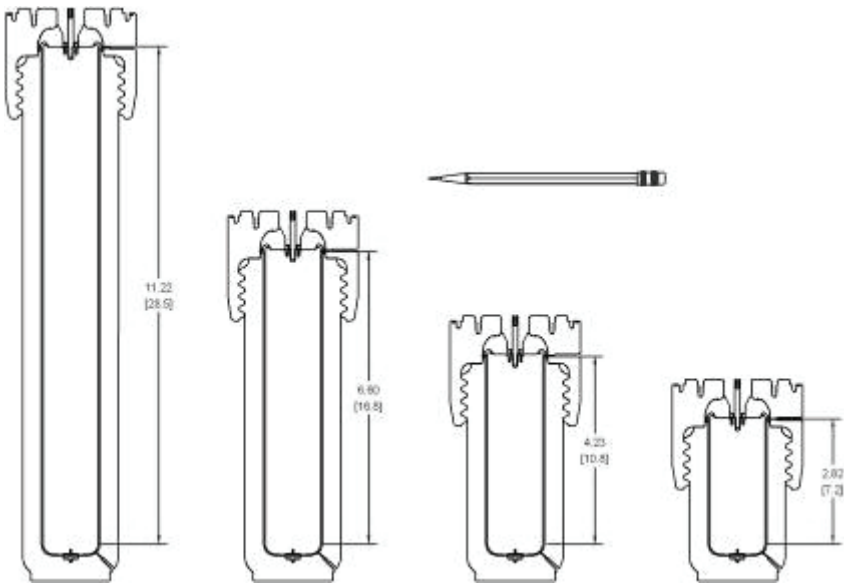

Figure 6. Preliminary mechanical oscillator layouts

The PSpice model shown in Figure 5 was varied to incorporate the different coaxial section lengths illustrated in Figure 6. The simulated ringing waveforms for each oscillator frequency are given below in Figure 7 through Figure 10.

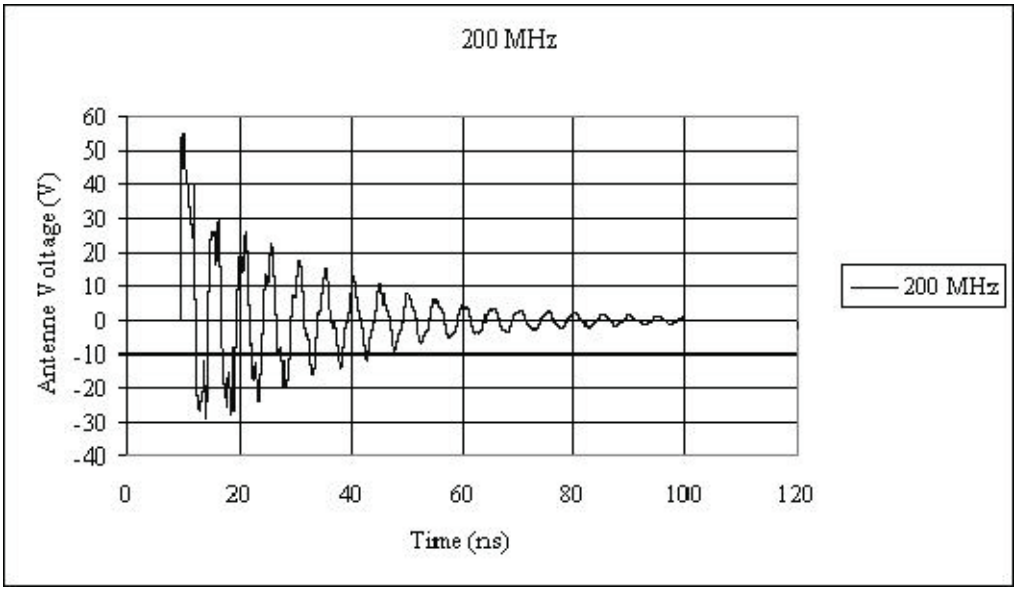

Figure 7. 200 MHz simulated waveform

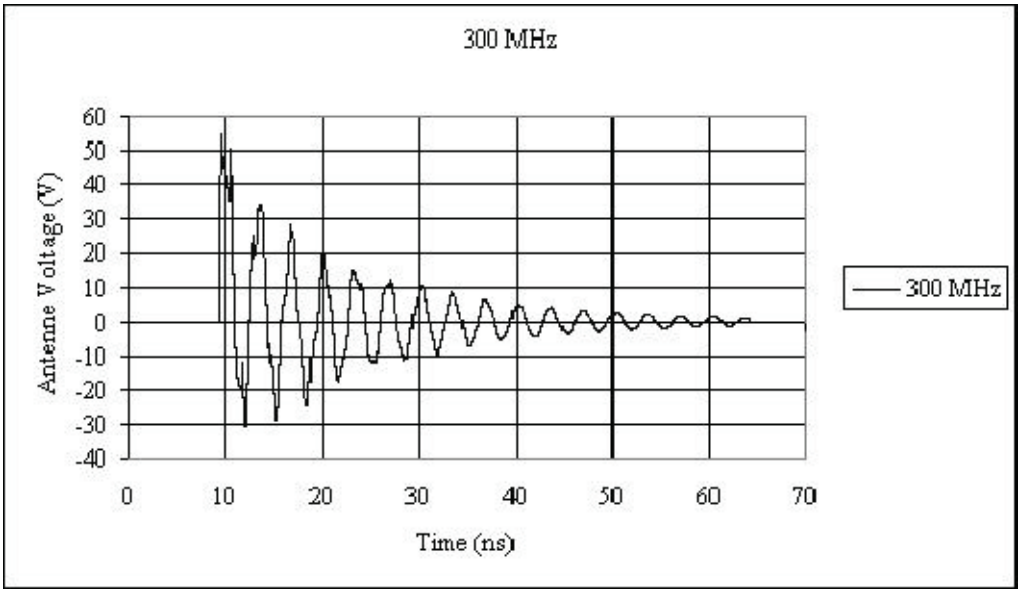

Figure 8. 300 MHz simulated waveform

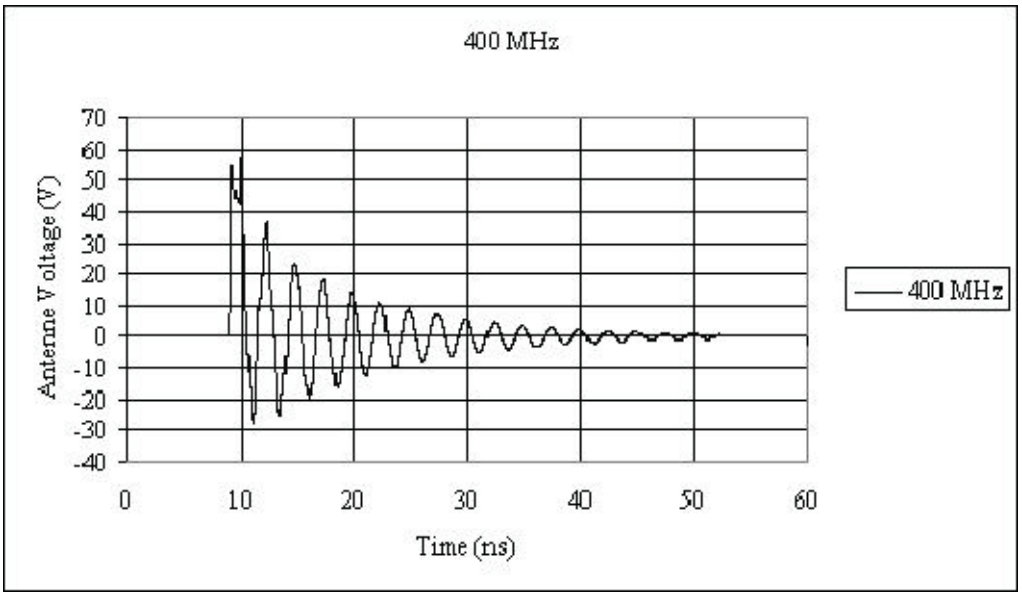

Figure 9. 400 MHz simulated waveform

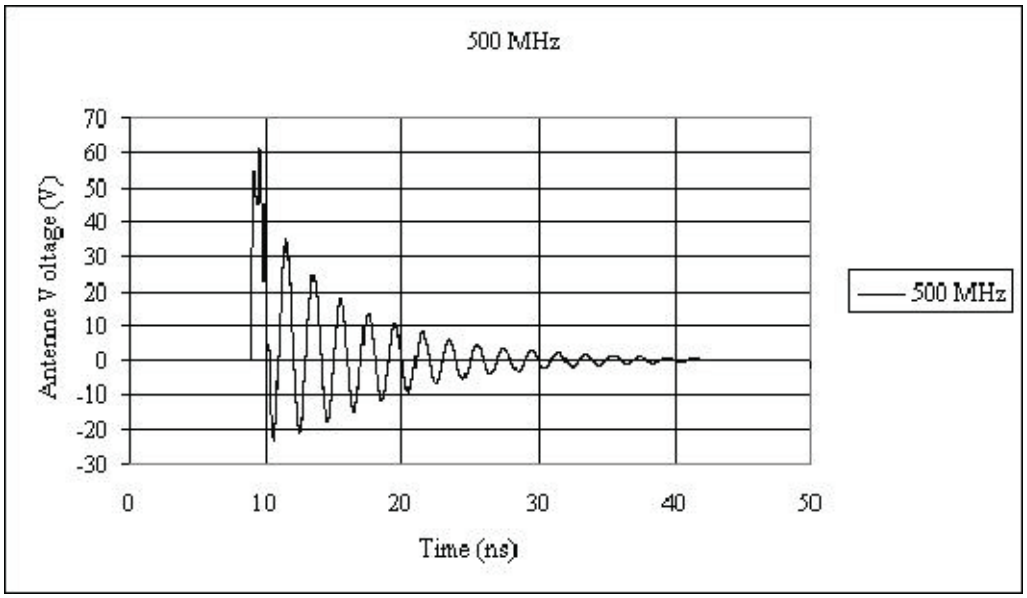

Figure 10. 500 MHz simulated waveform

These simulations are limited in scope, but they should reflect the relative change in ringing waveforms between the different configurations. It is noted that the voltage into a high-impedance load is seen to be nearly twice that of the charge voltage, as the transmission line theory requires.

3.3 Simulations of Electric Fields within the 200 MHz Oscillator

The magnitude of the electric field distribution along the surface of the inner conductor of the 200 MHz oscillator is shown below for an assumed 30 kV charge. The details near the switch and RTL are shown in Figure 11. The overall oscillator magnitude electric fields are shown in Figure 12.

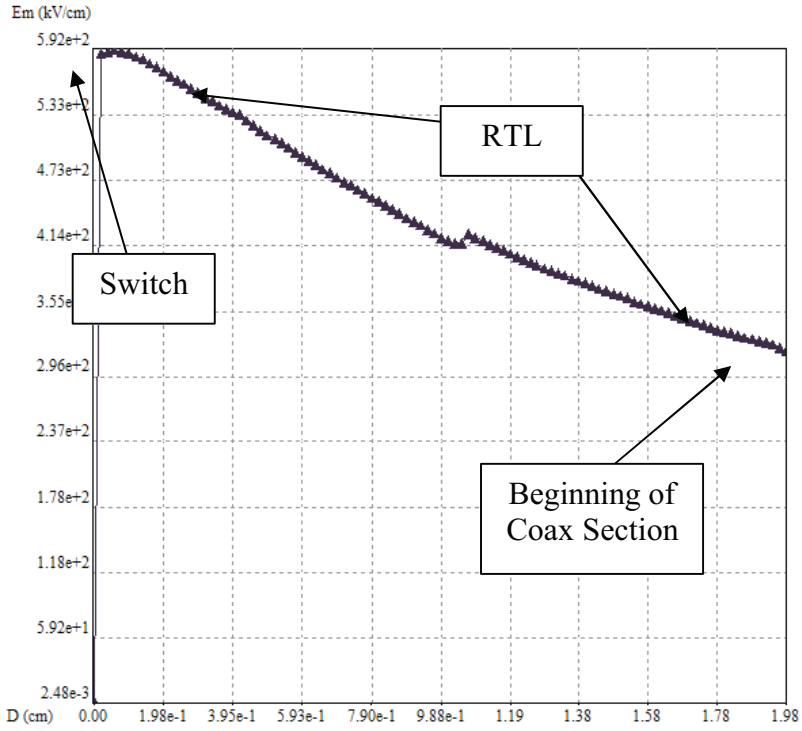

Figure 11. Magnitude electric field distribution in 200 MHz oscillator (detail)

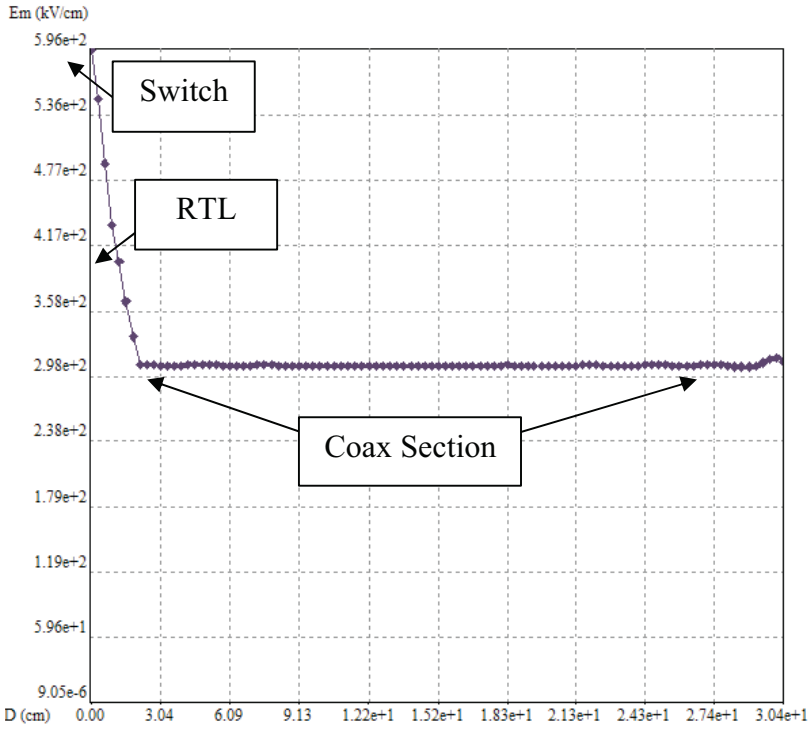

Figure 12. Magnitude electric field distribution in 200 MHz oscillator (entire)

As can be seen in Figure 12, the electric fields gradually decrease from approximately 600 kV/cm or 60 MV/m in the switch section to approximately 300 kV/cm or 30MV/m in the oscillator section. The electric field distribution indicates that the switch will operate at approximately 300 psig nitrogen for 30 kV charge voltage. Approximate operating pressures for nitrogen is given in Table 1.

Table 3. Approximate operating pressures for nitrogen insulation

Voltage (kV)	Field (kV/cm)	Approx Pressure (psig)
5	98.0	33
10	196.1	81
15	294.1	129
20	392.2	177
25	490.2	225
30	588.2	274

The above design is conservative electrically and the source should repeatedly switch in the switching section, as opposed to the oscillator section. If it is desirable to increase the Q of the oscillator, the overall outer diameter of the oscillator can be reduced (maintaining the same impedance level) to reduce the overall length of the RTL. The trade-off in doing this is that there will be more frequent erroneous switching events (switching events that occur in the coaxial section). It is not possible to accurately characterize the increased frequency of erroneous switching events, but going to 450 kV/cm (75% of switch fields) in the oscillator section is reasonable if we need more Q.

The initial electrical designs indicate that all four oscillators would operate at a 30 kV charge voltage, and perhaps to as high 60 kV, if desired. It appears that the cylindrical oscillator provides the best combination of performance and straightforward scalability.

The electrical simulations also indicate that all four oscillators can be made to ring at the desired center frequencies. Given the small switching gap, it is necessary to maintain accurate fabrication techniques, as the ring frequency depends strongly on the conductor spacing in the RTL.

The operating pressure for the 30 kV charge voltage will be approximately 300 psig nitrogen. The oscillator Q can be increased if desired, but the trade-off will be increased numbers of erroneous switching events in the coaxial section, as mentioned previously.

4. Fabrication of the Switched Oscillators

In the previous section, we have described the design features of 4 switched oscillators. Of these 4 designs, two have been fabricated. They have designed center frequencies of 200 MHz and 500 MHz, and are the longest and the shortest of the 4 oscillators shown in Figure 6. The fully assembled oscillators are shown in Figure 13.

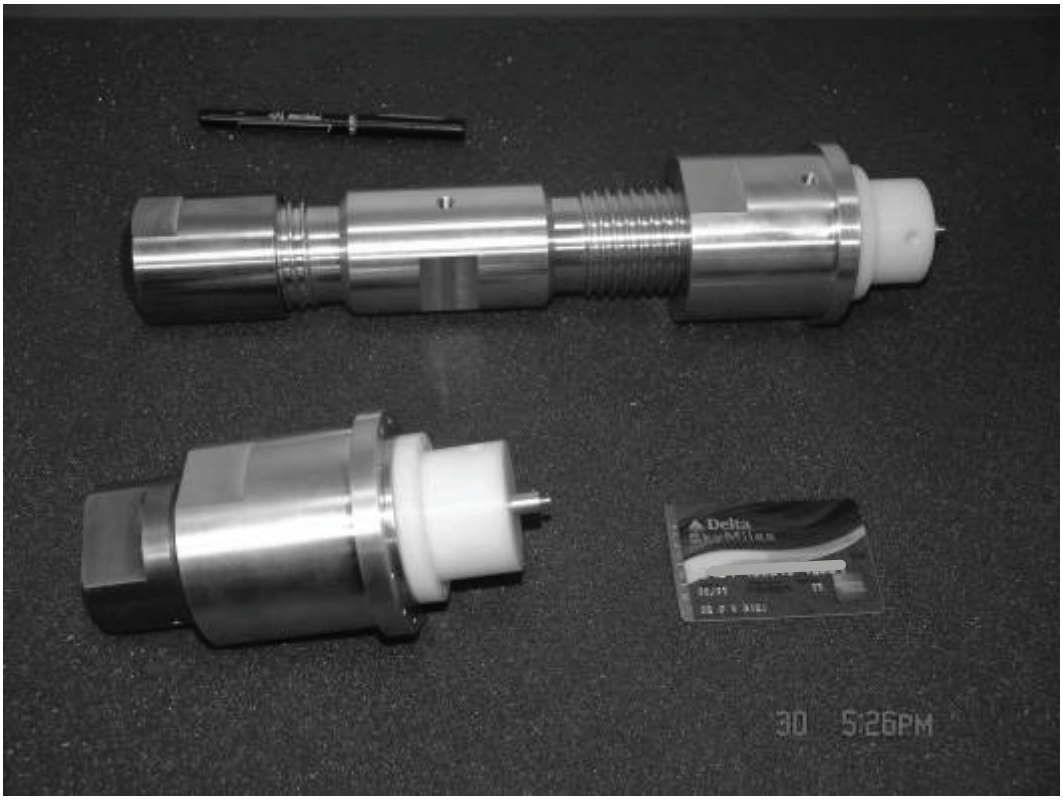

Figure 13. Switched oscillators (200 MHz top) and 500 MHz (Bottom)

We have used copper tungsten surfaces in the switch region, as can be seen in Figure 13. There is also an oil dome at the top of the oscillator and the hot electrode can be seen to be protruding out of the oil dome. The switched oscillators were initially tested with a 100 Ω dummy load which is really a finitely wide plate above a ground plane. This arrangement can be seen in Figure 14 below.

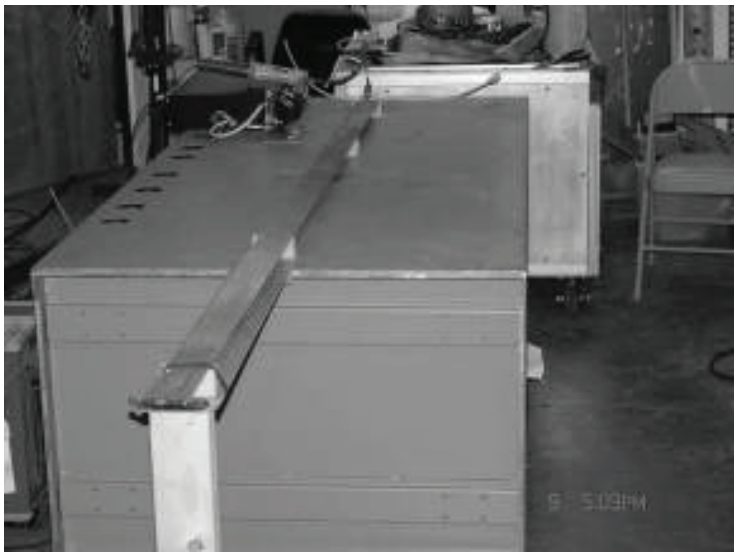

Figure 14. Switched oscillators tested into a 100 Ω dummy load transmission line

The connection between the switched oscillator and the top plate of the transmission line via a blocking capacitor is shown in Figure 15 and the location of a capacitive divider to measure the field on the ground plane can be seen in Figure 16.

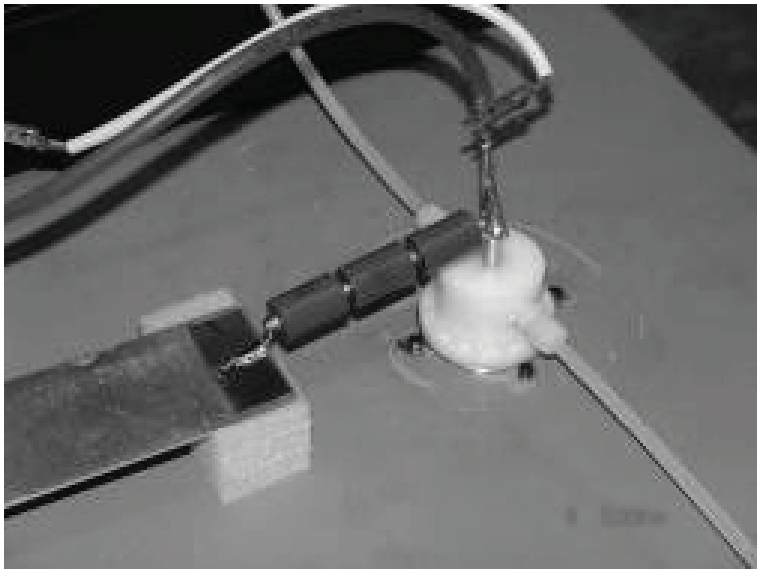

Figure 15. Source/load connection

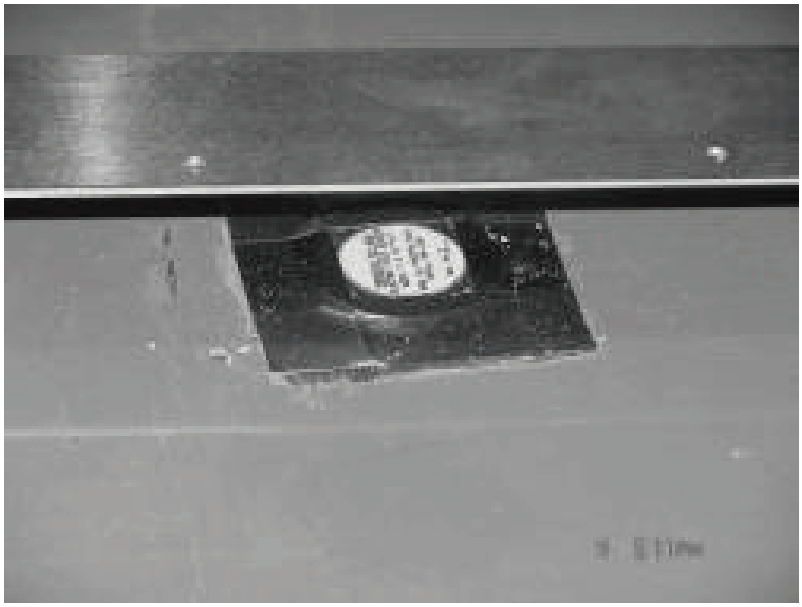

Figure 16. Field measurement

The measured electric field in the ground plane (in arbitrary units) is shown in Figure 17 and Figure 18 for the 200 MHz and the 500 MHz oscillators.

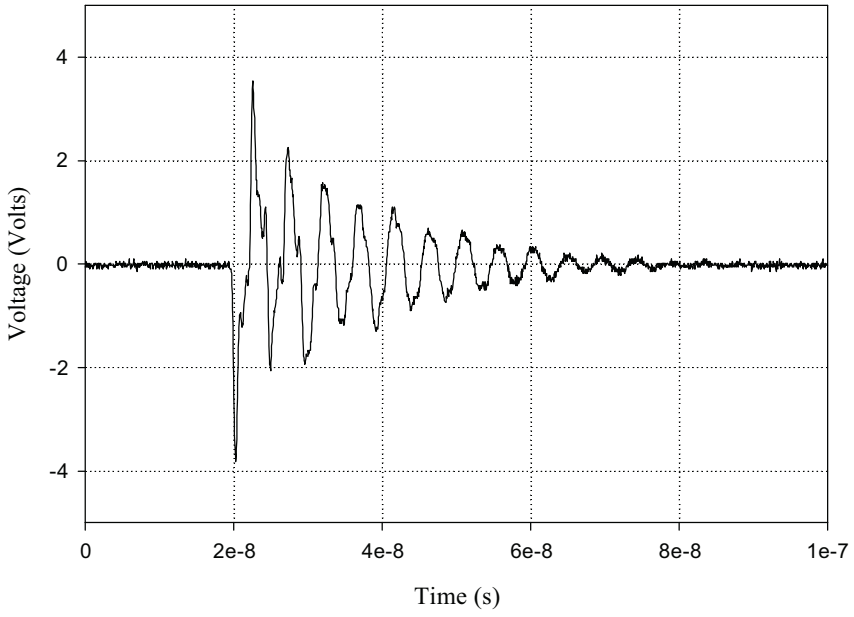

Figure 17. The electric field on the ground plane for the 200 MHz oscillator into a 100 Ω transmission line

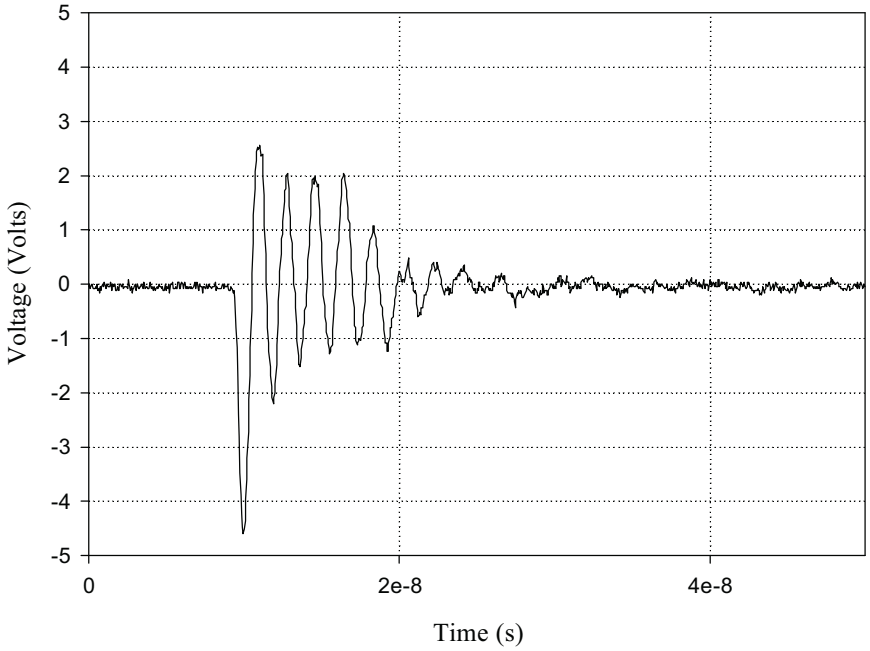

Figure 18. The electric field on the ground plane for the 500 MHz oscillator into a 100 Ω transmission line

The measurements shown in Figures 17 and 18 compare well with the PSpice simulations in Figures 7 and 10. The spectral electric field corresponding to the temporal measurements above are shown in Figures 19 and 20.

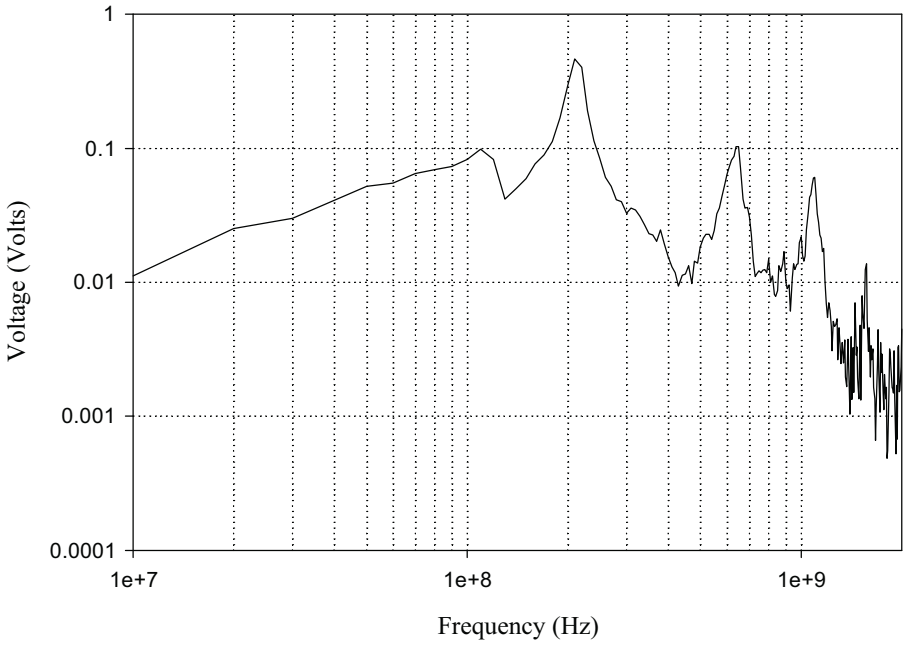

Figure 19. Magnitude of the electric field spectrum at 200 MHz

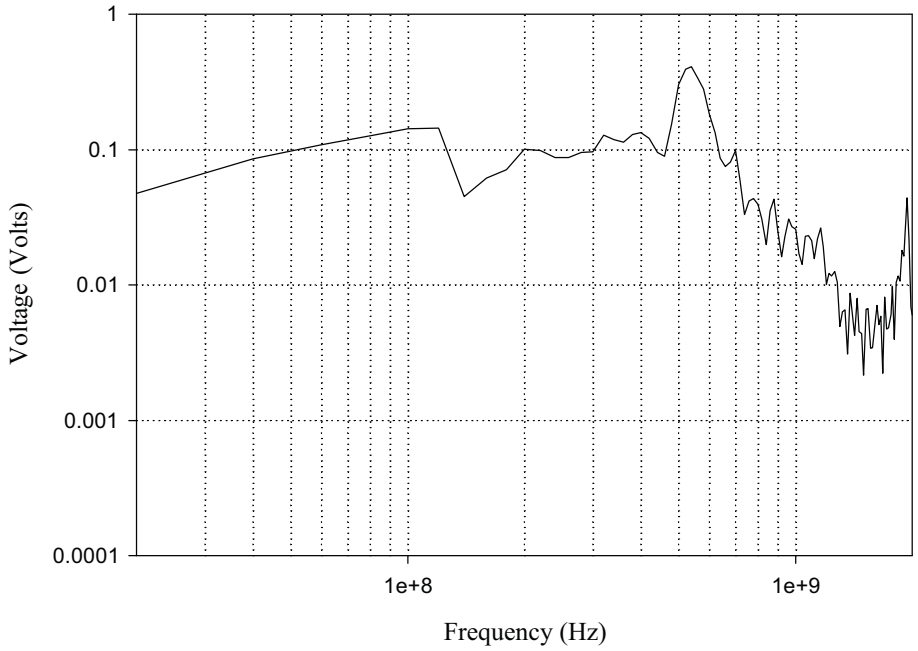

Figure 20. Magnitude of the electric field spectrum at 500 MHz

The above results of the dummy load tests confirms that the switched oscillators are working as expected and they have a Q of ~ 12. We can now proceed to integrate these oscillators into suitable antennas and measure the radiated waveforms.

4.1 Battery Operation of the Switched Oscillators

A Controlled **P**ulse **G**enerator (CPG-35kV) unit is designed to charge capacitive loads on the order of 200 pF to a voltage that is adjustable from 0 to 30 kV in 60 μs. Both the switched oscillators (200 and 500 MHz) can be driven by this unit. The system is self contained and requires no external power source after the internal 12 V battery is charged.

The CPG consists of the following components (see Figure 21):

- Coil driver unit (CDU)
- Pulse transformer or the ignition coil from a FORD automobile (selected after Experimenting with a few coils)
- Pulse transformer harness
- Fiber optic control cable
- Hand-held Master control unit (MCU)
- Battery charger

The pulse transformer is connected to the user provided capacitive load. The output is typically connected to the capacitive load through some type of isolation resistance. The pulse transformer is driven by the coil driver unit (CDU). The driver unit applies a 0-500 volt pulse

to the pulse transformer. The driver unit is controlled by the master control unit (MCU) via a fiber optic cable. The MCU allows the selection of burst length and pulse repetition frequency (PRF).

Figure 21. Various components of the CPG-35kV system

The design philosophy of the CPG is schematically shown in Figure 22.

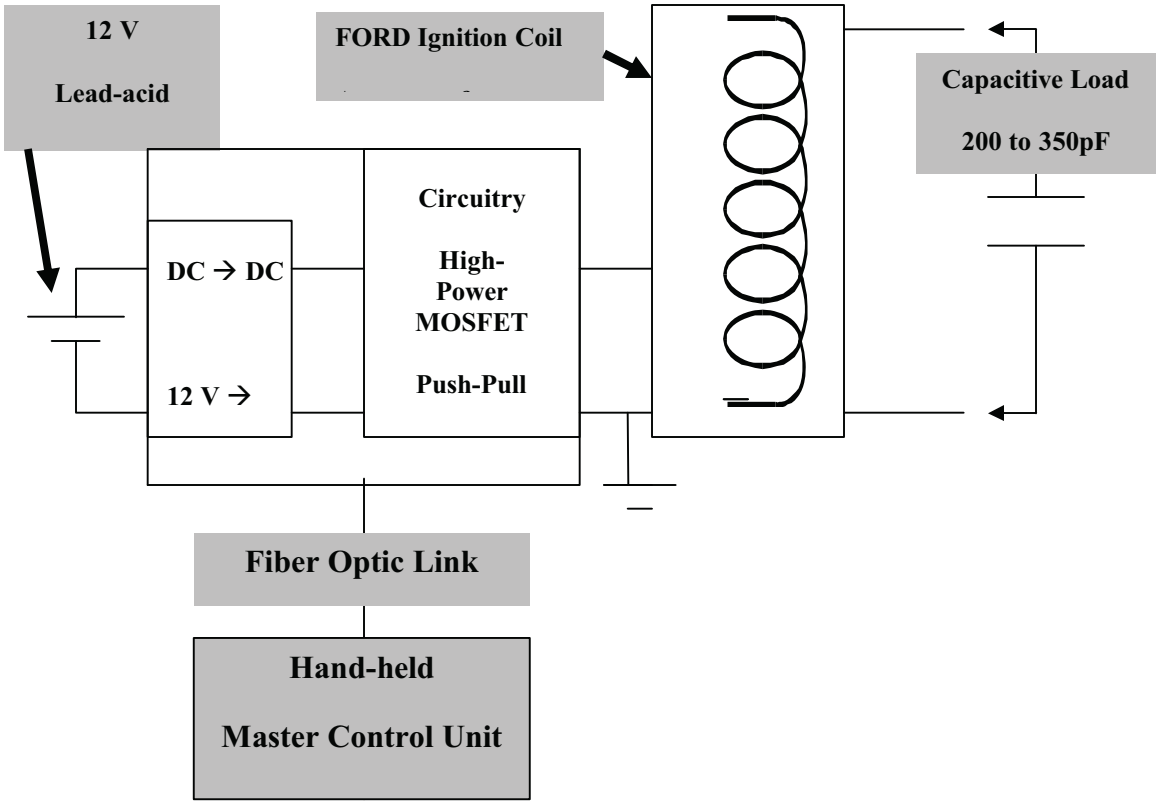

Figure 22. Block-schematic of the system

The CPG design may be explained as follows. We start with a 12 V rechargeable, lead-acid battery. This voltage is stepped up to 500 V using a DC to DC converter. The voltage output of the DC to DC converter is controlled by a knob. This is then followed by a pair of high-power MOS-FET transistors, which converts this 500V DC voltage into rectangular pulses. The DC to DC converter and the circuitry are contained in a black box called the Coil Drive Unit (CDU). This CDU is fiber-optically linked to a hand-held Master Control Unit (MCU). In the MCU, the pulse width is set at 60 μs, the PRF and the number of pulses is selected by the user. The PRF can be varied from 1 to 10Hz while the number of pulses can be selected between 1 to 250 pulses. These two settings together then control the burst length. For example, selecting 200 pulses at 10 Hz will result in a burst length of 20 seconds.

This unit makes the switched oscillator an autonomous source, which can be integrated with a passive helical antenna described in the next section.

5. Computed Responses of the Helical Antenna

We have used the 500 MHz switched oscillator to provide transient energy to a helical antenna, which is shown in Figure 23. This is a standard helix antenna that is designed to operate at a frequency around 500 MHz. Normally such antennas are used for communications purposes using relatively narrowband excitations. For the present application, however, the antenna is driven by a transient voltage source having a wider bandwidth, and as a consequence, the antenna behavior is different from that normally expected for the helix under narrowband excitations.

The helix shown in Figure 23 was procured from M2 Antenna Systems, Inc., in Fresno, California. This antenna has the following electrical parameters listed in Table 4.

Figure 23. Illustration of the helical antenna and the associated octagonal ground plane

Table 4. Helix Antenna Parameters

- Major diameter (D) center to center = 19.05 cm
- Circumference (C) = 3.1415 x D = 59.845 cm
- Minor diameter ($2r$) = 9.525 mm
- Minor radius (a) = 4.7625 mm
- Spacing between adjacent turns (S) = 13.335 cm
- Length L of one turn = 61.313 cm
  (L is approximately one wavelength at 500 MHz)
- Free-space wavelength at 500 MHz = 60 cm
- Number of turns N = 10
- Total axial length $L_t = N\,S = 10\,S$ = 1.3335 m
- Pitch angle θ_p = arctan (S/C) = 12.56°
- Ground plane is an octagon made from a square metal plate with dimensions 55.88 cm x 55.88 cm. It is approximated by a circle of radius r_g = 27.94 cm.

5.1 The Excitation Voltage

The output voltage of the oscillator into the 100 Ω load can be modeled adequately by an exponentially damped sine wave of the form

$$V(t) = Ae^{-\alpha(t-t_s)} \sin\left(2\pi f_o (t-t_s)\right)\Phi(t-t_s) \tag{4}$$

where f_o is the oscillation frequency of 500 MHz, t_s is an arbitrary time shift or "start time" of the waveform, and α is the damping constant of the waveform given by

$$\alpha = \frac{\pi f_o}{Q} \tag{5}$$

The parameter Q is the *quality factor* of the signal. Typically, for HPEM sources the value of Q can range from 1 to 100, depending on the losses in the oscillator and the nature of the load resistance. The term $\Phi(t-t_s)$ is the unit step function that turns on at $t = t_s$.

The amplitude term A in Eq.(4) is

$$A = V_{peak} \frac{\left(1+\left(\frac{\alpha}{2\pi f_o}\right)^2\right)^{1/2}}{\exp\left(-\frac{\arctan(2\pi f_o/\alpha)}{2\pi f_o/\alpha}\right)} \tag{6}$$

where V_{peak} is the peak value of the waveform.

For the present calculations, we assume that V_{peak} = 50 kV, and this value will need to be verified in the measurements.

The Fourier spectrum of the waveform in Eq.(4) can be determined analytically to be

$$\tilde{V}(\omega) = A\frac{2\pi f_o e^{-j\omega t_s}}{(2\pi f_o)^2 + (j\omega+\alpha)^2} \tag{7}$$

Figure 24 presents the 500 MHz damped sine waveform and spectral magnitudes for different values of the Q parameter, which range from 1 to 50. It is estimated that the Q = 10 value will be closest to that of the actual source feeding the helix antenna, but this conjecture remains to be validated in the measurements.

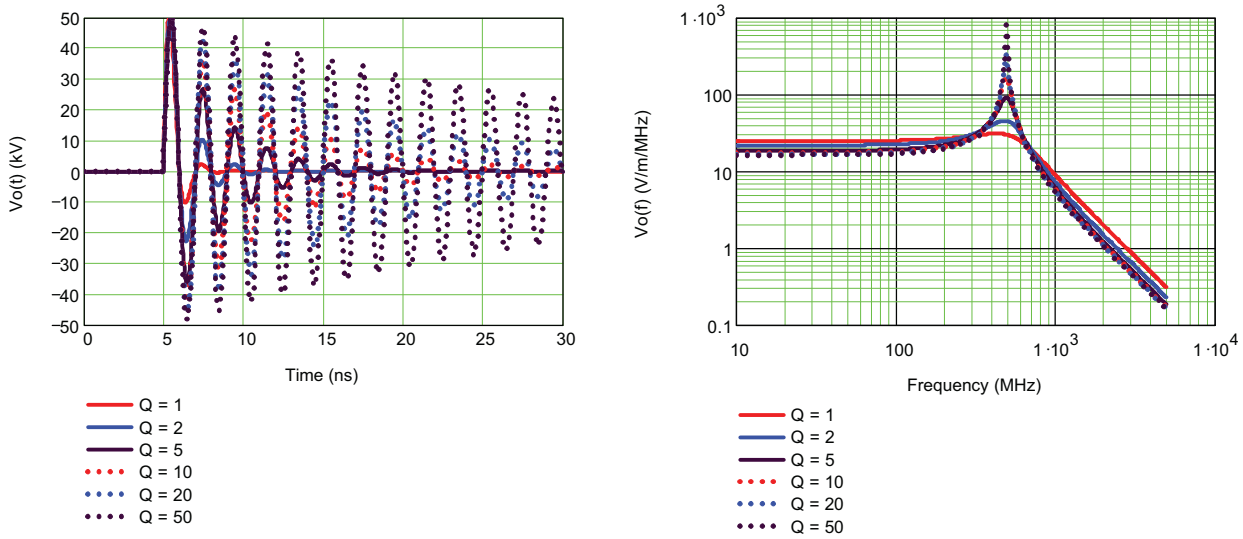

a. Transient response

b. Spectral Magnitude

Figure 24. Illustration of the 500 MHz damped sine waveform and spectral magnitude for different values of Q.

5.2 Wideband Input Impedance

Using the helix parameters provided in Table 4, a wide-band antenna model was developed for use with the WIPL-D computer code [6]. The model is shown in Figure 25 and consists of a 10-turn thin wire antenna mounted over a circular flat conducting plate having a radius commensurate with the dimension of the octagonal ground plate shown in Figure 23.

This antenna is assumed to be excited by a lumped unit-amplitude voltage source at the helix/ground plane interface. The calculation of the antenna response using WIPL permits an estimation of the input impedance of the antenna, together with the radiated EM fields from the antenna.

The computed input impedance of the helix antenna is shown in Figure 28. At low frequencies (below about 350 MHz) there are the usual resonances similar to those of a wire dipole antenna. Above this frequency, there is a range of frequencies for which the impedance is relatively constant, and this is the usual frequency range used for helical antennas. At the target frequency of 500 MHz, the input impedance is $Z_{in} = 118 - j\ 55\ \Omega$.

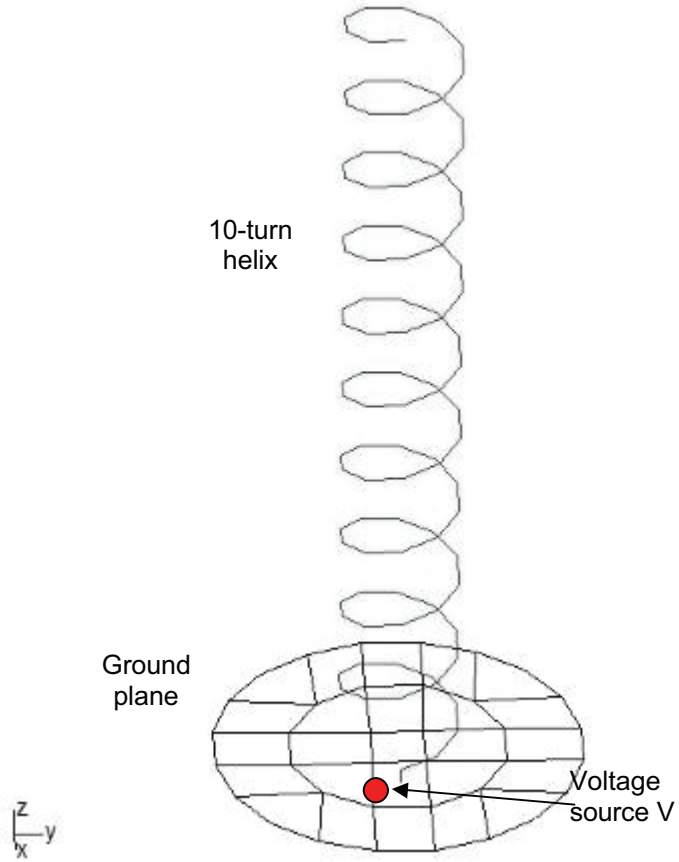

Figure 25. WIPL model of the 10-turn helix antenna with the ground plane and lumped voltage excitation source.

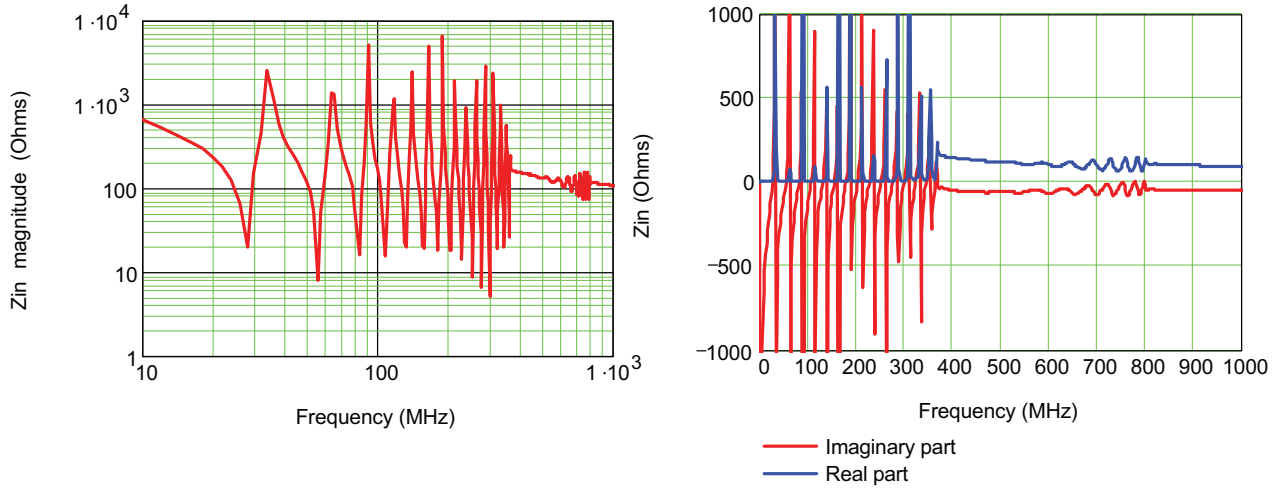

a. Magnitude b. Real and Imaginary Parts

Figure 26. Plots of the magnitude and real and imaginary parts of the input impedance of the helical antenna, shown as a function of frequency

5.3 The On-Axis Radiated E-field Spectrum

Figure 27 shows the coordinate system for calculating the radiated fields. From a detailed analysis of this and other helices, it is found that in the vicinity of the design frequency (500 MHz in the present case), most of the EM energy is radiated in the boresight of the antenna where $\theta \approx 0°$, as opposed to the broadside radiation for the antenna at the lower frequencies where the antenna operates like a vertical dipole.

The WIPL-D code computes both of these E-field components in the radiation zone in *normalized* form rE_θ/V and rE_ϕ/V, where r is the range form the antenna origin to the field observation location. These expressions are complex-valued transfer functions that relate the distant E-fields to the excitation voltage at a particular frequency f. These calculations are performed for a wide range of frequencies, and the spectral responses for the normalized E-fields rE_θ and rE_ϕ can be determined by multiplying the transfer functions by the damped sine spectrum of Eq.(4). The resulting normalized fields then can be divided by any specific range r, to provide the actual E-field spectra at the field observation point. Finally, an inverse FFT of these spectra provide the transient responses.

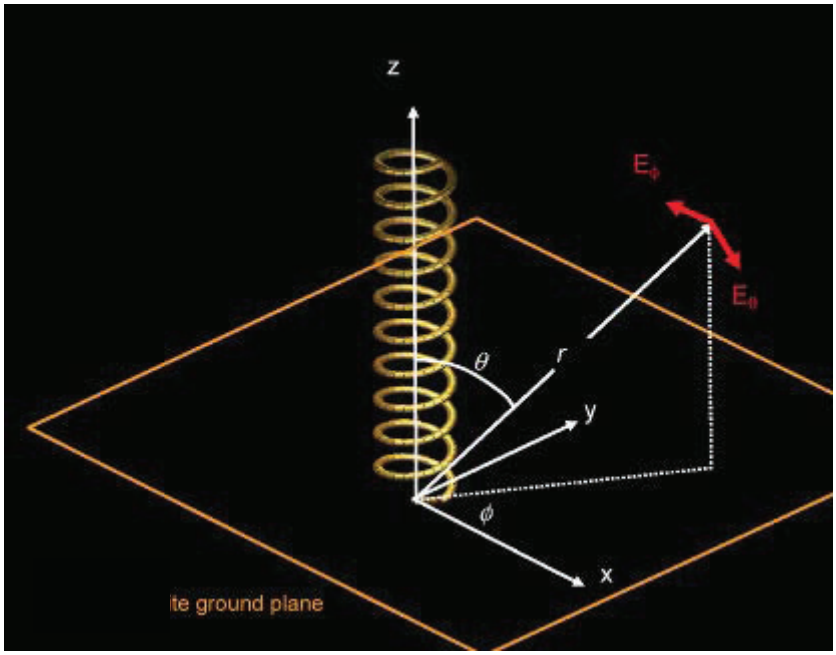

Figure 27. Coordinate system for the radiated fields

As an example of the radiation field of the 10-turn helix, Figure 28 shows plots of the normalized radiation patterns $|rE_\theta/V|$ and $|rE_\phi/V|$ as a function of frequency for an observation point located along the axis of the helix, at $\theta = 0$. Note that in the resonance region (f < 300 MHz) the E_θ and E_ϕ components have different magnitudes, indicating that the field is elliptically polarized. Near the operating frequency of about 400 – 500 MHz, however, the field component amplitudes are nearly real, and a close examination of the phase shows that the field is nearly circularly polarized in the boresight direction.

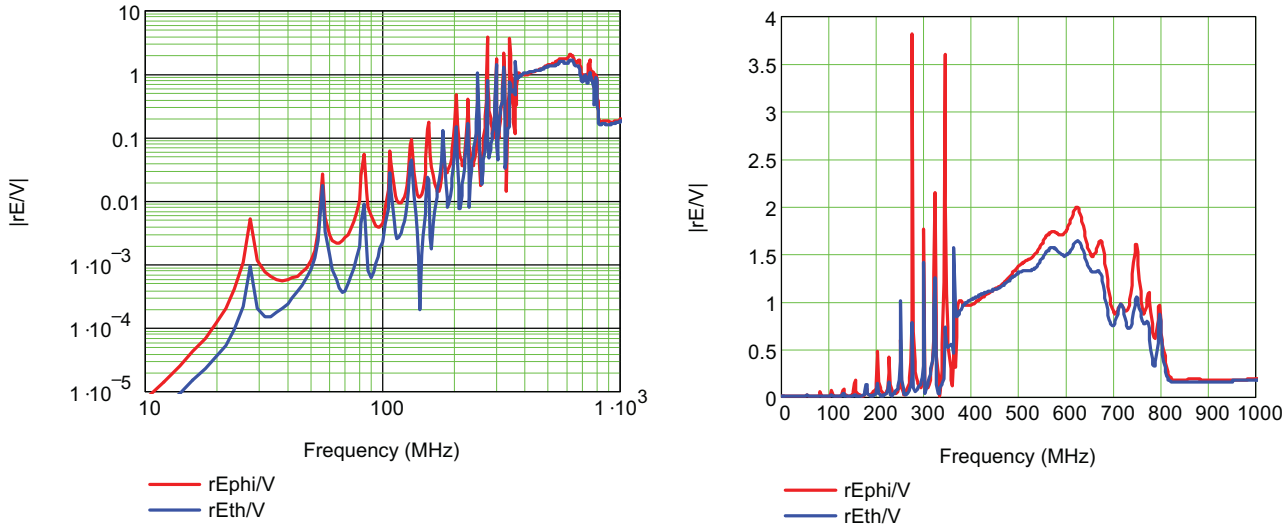

a. Log-log plot b. Linear plot

Figure 28. Plots of the far-field transfer function magnitudes $|rE_\theta/V|$ and $|rE_\phi/V|$ in the boresight direction for the 10-turn helical antenna, shown as a function of frequency

5.4 Computed on-Axis Broadband and Transient Responses

Multiplying the radiated field transfer functions of Figure 28 by the voltage excitation spectrum for the waveform in Eq.(7) with Q = 10 provides the range-normalized response spectrum (rE) shown in Figure 29. These plots show the spectral magnitudes of the θ, ϕ and *total* field components as a function of frequency, and are plotted on both log and linear plots. In this case, the total field is the root-sum-square (RSS) value of the θ and ϕ field components, given as $E_{total} = \sqrt{|E_\theta|^2 + |E_\phi|^2}$. Note that the units of these plots are in (Volts/MHz).

In examining the spectra in Figure 29 we note that the largest spectral content occurs at 500 MHz. This is due to the peak in the excitation spectrum. Thus, it is expected that the transient response for the radiated E-fields will be very similar to a damped sine at this same frequency.

By taking an inverse Fourier transform of the spectra in Figure 29, the transient responses for magnitudes rE_θ (t) and rE_ϕ (t) can be computed. Both the late- and early-time waveforms are shown in Figure 30 for Qs of 1, 10 and 100.

It is observed that the temporal radiated fields exhibit a growth (for one or 2 cycles) before decay. It may be explained as follows. As the current starts to flow on the first turn of the helix, the radiation occurs. The radiation from the current on the second turn adds causing the total radiation to grow. Then the current on the subsequent turns radiate, but since the current is decaying, the radiated fields start to decay as well. Form the results of Figure 30, we observe that the values of $rE_{peak}(t)/V(t)$ are (0.56 for Q =1) and (1.624 for Q =10). In estimating the $E_{peak}(t)$, we have considered the vector sum of the two components.

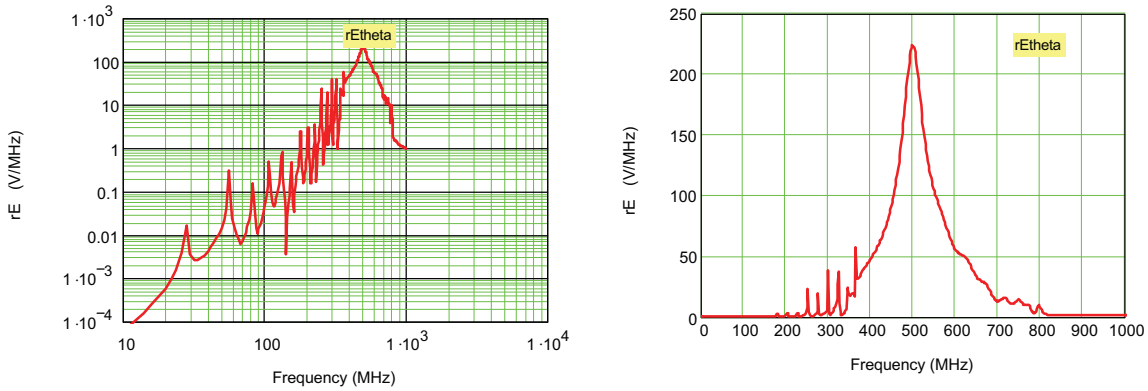

a. θ-component

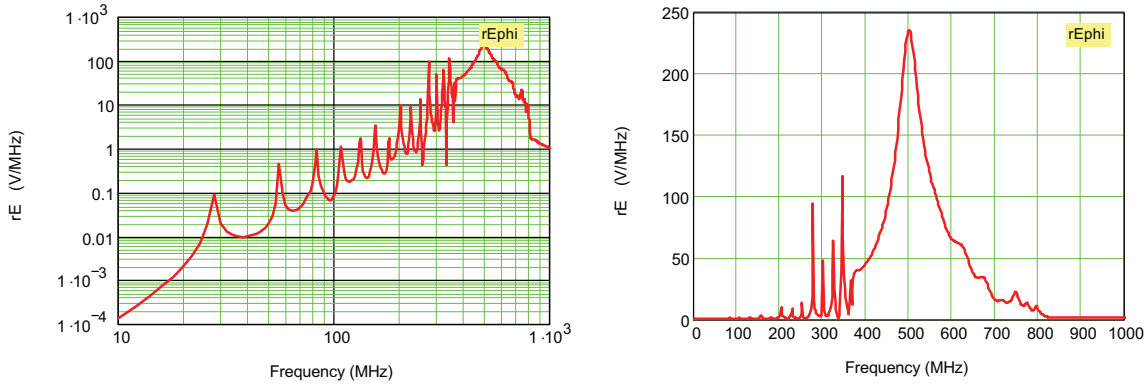

b. ϕ-component

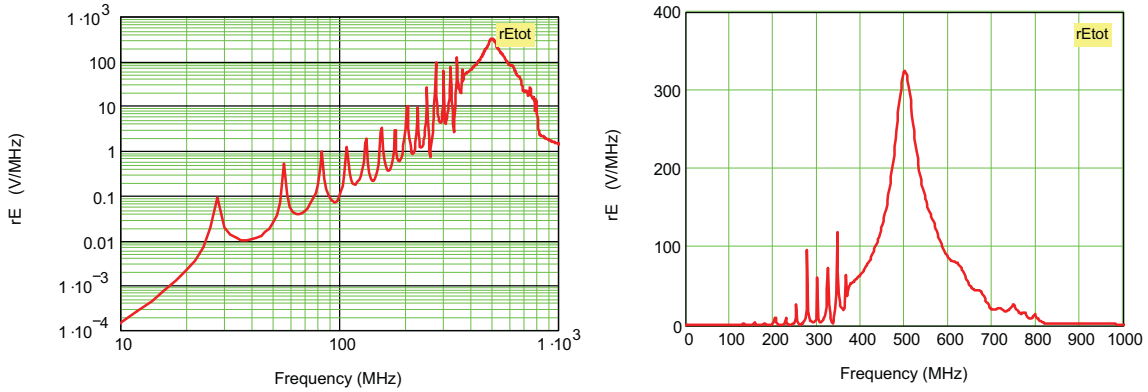

c. Total field component

Figure 29. The range-normalized spectral magnitudes for the E_θ, E_ϕ and E_{total} field components for the helix antenna and a 50 kV voltage excitation waveform with Q = 10. (The data presentation is in both log-log and linear formats.)

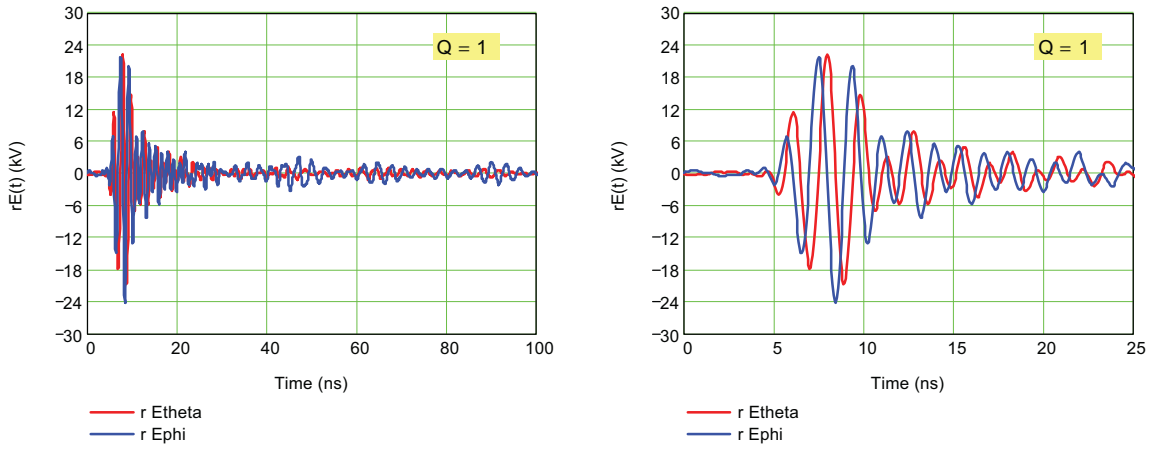

a. Q = 1

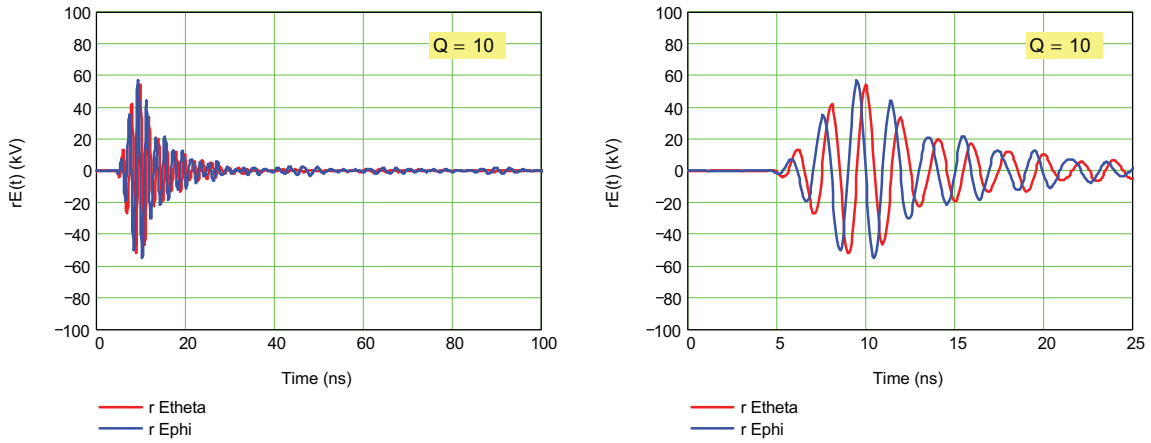

b. Q = 10

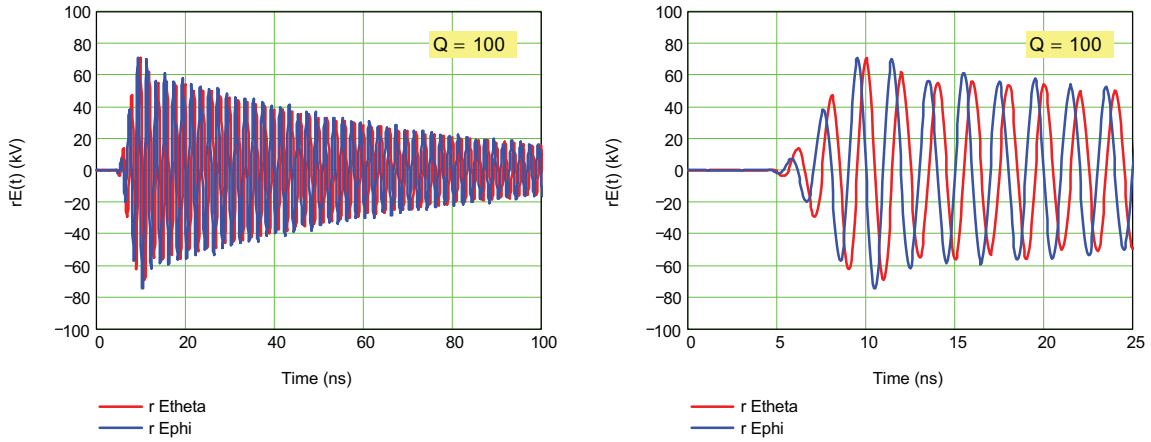

c. Q = 100

Figure 30. Late-time and early-time waveforms depicting the on-axis range-normalized E_θ and E_ϕ field components for Qs of 1, 10 and 100.

5.5 Helix Response Variations with the Number of Turns

The 10-turn helix shown in Figure 23 is rather cumbersome, due to its long physical length. Thus, a study of how the radiated field varies if the number of turns is reduced would be of interest.

Figure 31 presents plots of the frequency variation of the on-axis θ and ϕ components of the E-field in normalized form, for different numbers of turns of the helix. In these plots, the frequency varies from nearly 0 to 1 GHz, and there is a clear reduction in the radiated field level as the number of turns is reduced.

To summarize these results at the design frequency of 500 MHz, it is convenient to use the total radiated E-field component to define a *field reduction factor* for the total radiated field transfer function $|rE_{total}/V|$ relative to the 10-turn case. Table 2 summarizes the behavior of the various components of the E-field transfer function as the number of turns varies. Also shown are the field reduction factor and the overall helix length. Of course, if these results are to be applied to a helix antenna designed for a different frequency f_1 (in MHz), the helix length L_o should be scaled as

$$L_1 = L_o \frac{500}{f_1}.$$

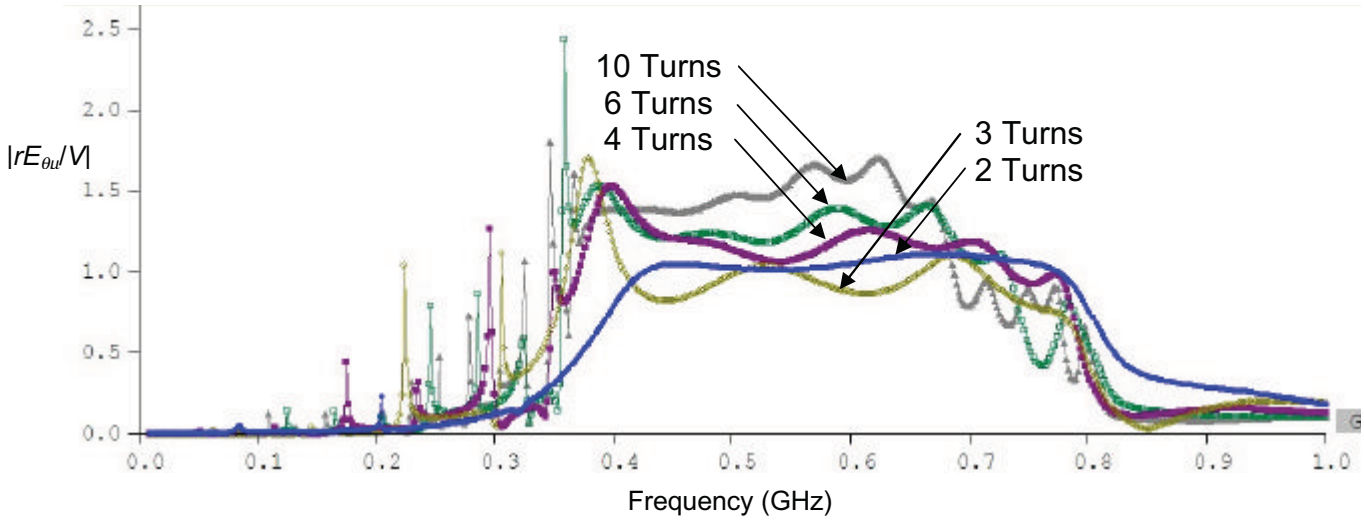

a. $|rE_\theta/V|$

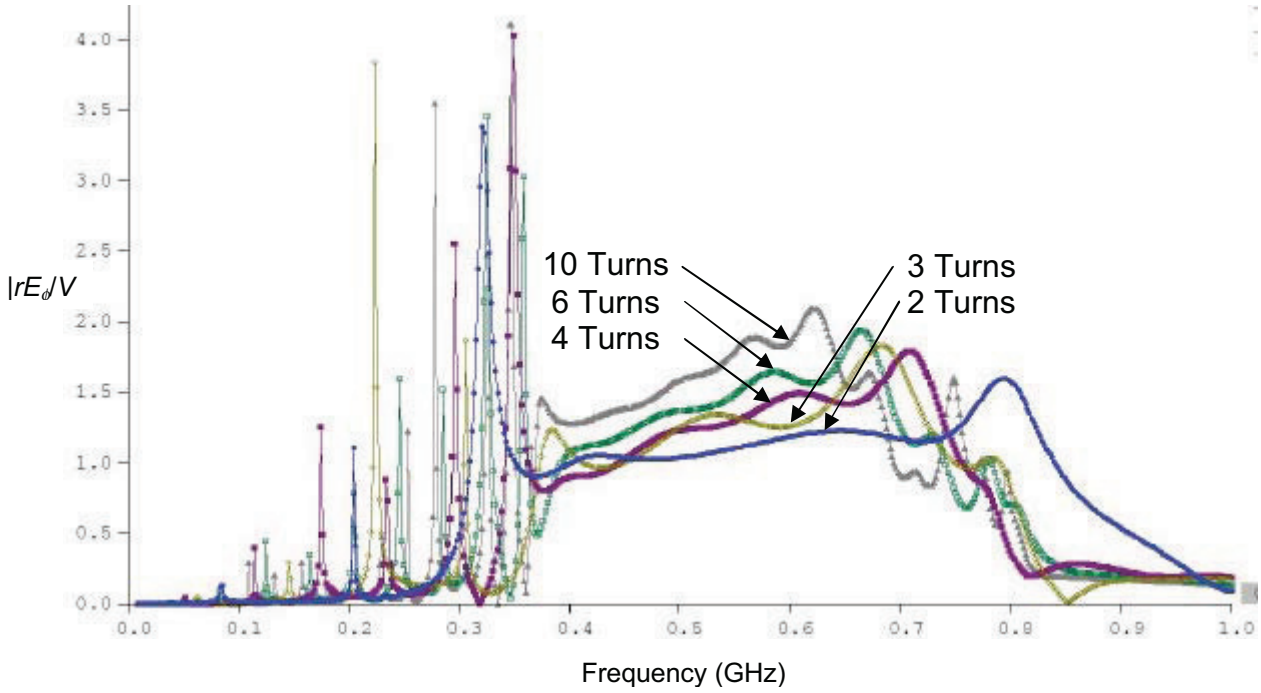

b. $|rE_\phi/V|$

Figure 31. Plots of the frequency dependence of the normalized on-axis radiation patterns $|rE/V|$ for the θ and ϕ components of the E-field, for different numbers of turns of the helix antenna. (Turns are indicated in the name of the data files in the plot.)

Table 2. Summary of the variation of radiated E-field with the number of turns of the helix antenna operating at 500 MHz.

Turns	$\lvert rE_\theta/V \rvert$	$\lvert rE_\phi/V \rvert$	$\lvert rE_{total}/V \rvert$	Field Reduction Factor†	Helix Length L_o (m)
2	1.02	1.03	1.45	0.67	0.27
3	0.975	1.22	1.56	0.72	0.40
4	1.15	1.21	1.66	0.77	0.53
6	1.23	1.35	1.82	0.85	0.80
10	1.47	1.56	2.14	1.0	1.33

† Field reduction factor is relative to the 10-turn case.

To visualize the data in Table 2, Figure 32 presents a plot of the field reduction factor and the antenna length for the 500 MHz helix, as a function of the number of turns. It is clear that if a small reduction of the radiated field level is permitted, the overall length of the antenna can be reduced significantly.

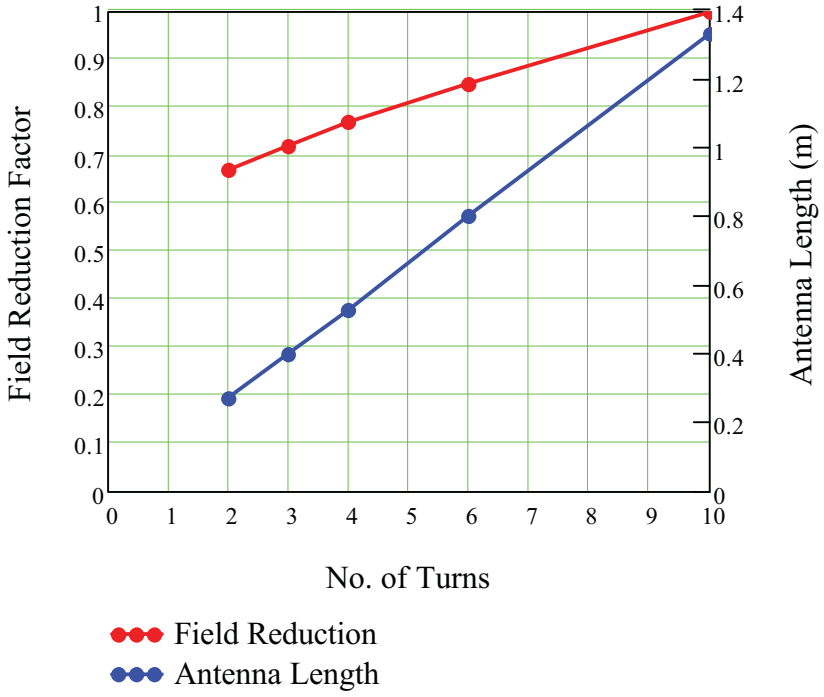

Figure 32. Plot of the field reduction factor and the antenna length for the 500 MHz helix, as a function of the number of turns.

5.6 Spatial Variations of the Radiation Pattern

All of the previous calculations for the helix antenna have concentrated on the radiation from the antenna in the axial direction. It is also interesting to examine the radiation in other directions. For the operating frequency of 500 MHz, Figure 33 presents the computed normalized radiation patterns $|rE/V|$ for both the θ and ϕ components of the E-field in the $\phi = 0$ plane. This is done for different numbers of turns of the helix antenna. Note that these data are presented as the actual values of $|rE/V|$, not in dB. Generally we note that as the number of turns decreases, the radiation pattern becomes broader and the field strength decreases, as previously seen in Figure 32.

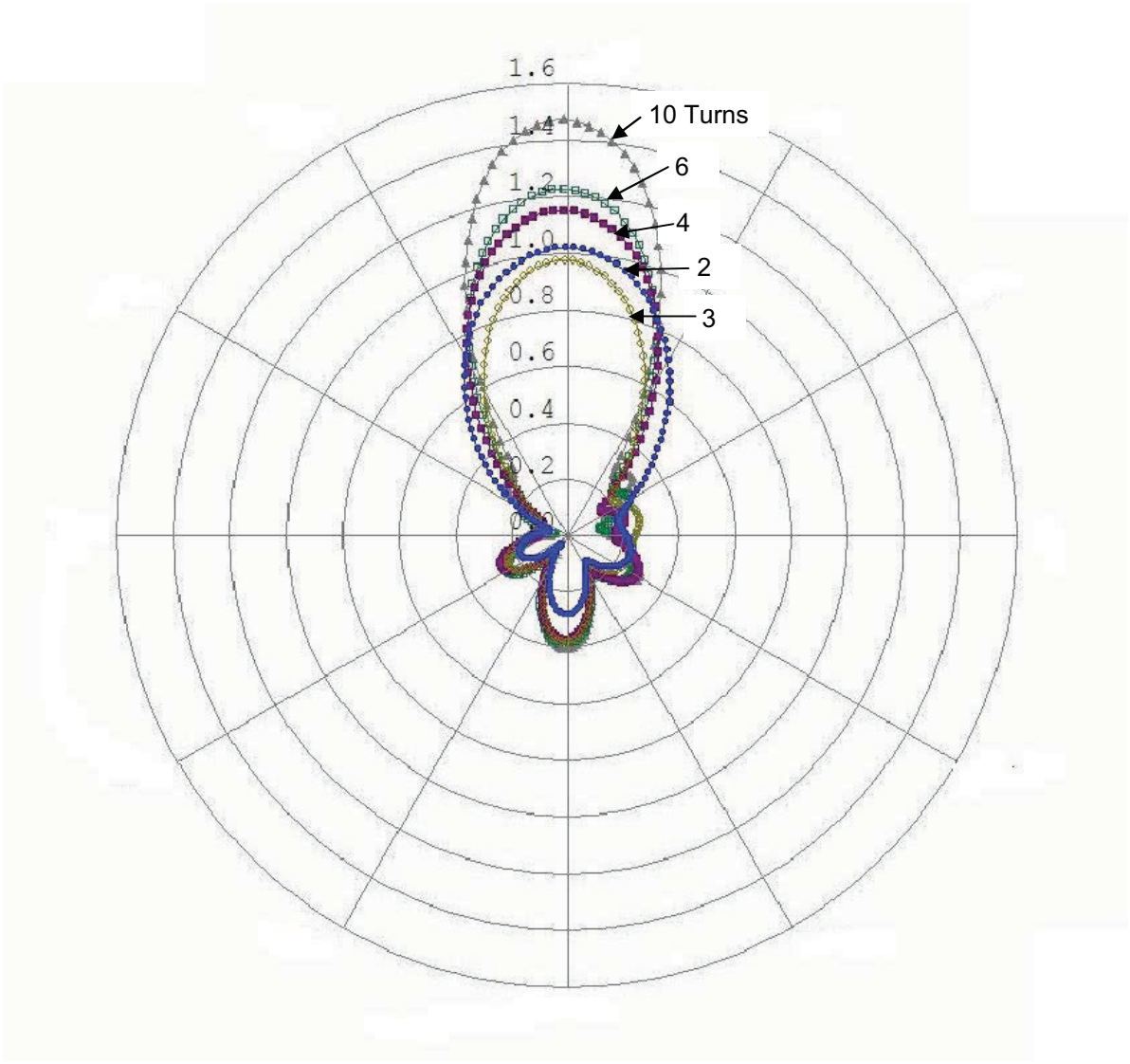

a. $|rE_\theta/V|$

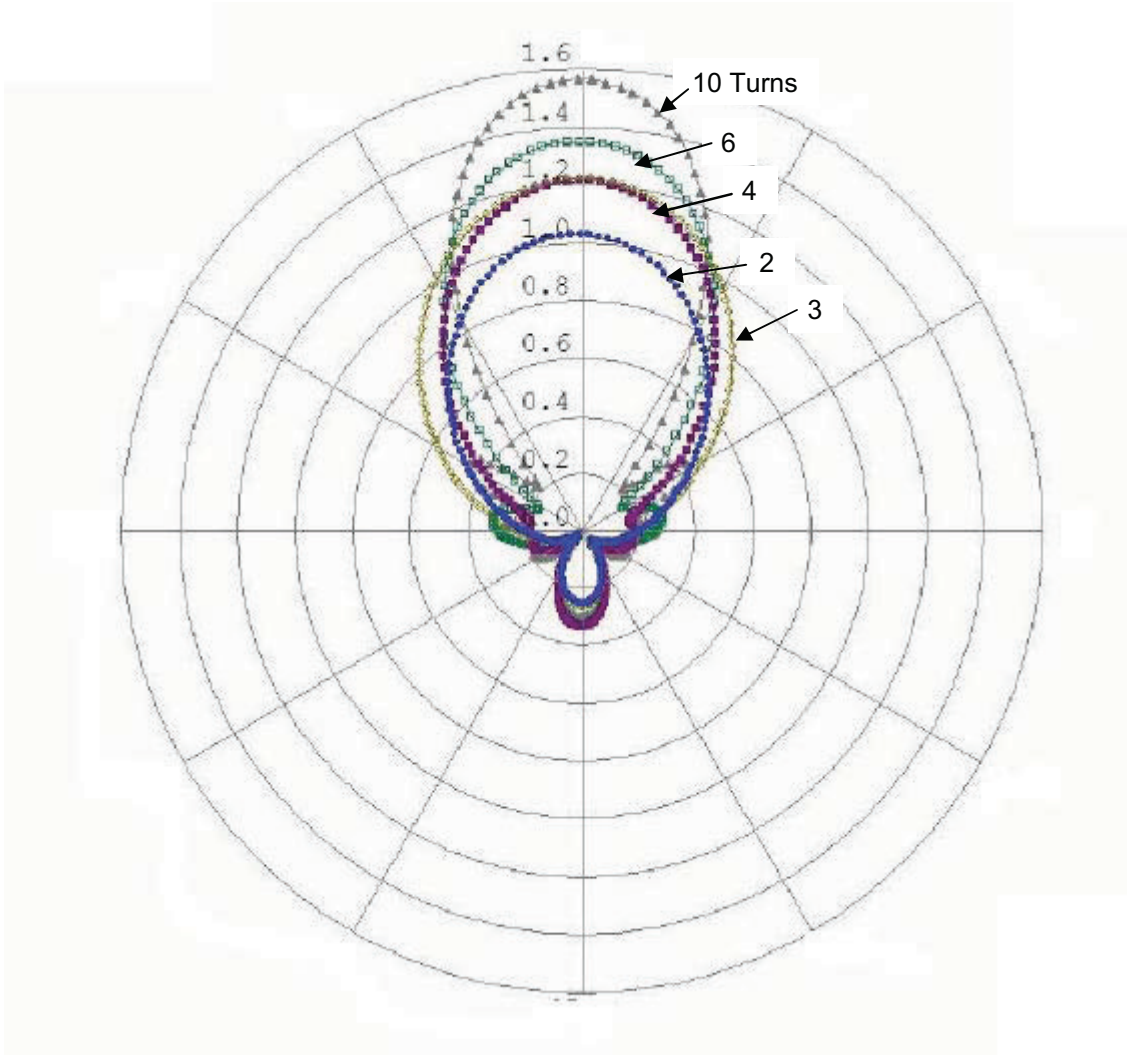

b. $|rE_\phi/V|$

Figure 33. Normalized radiation patterns $|rE/V|$ for the θ and ϕ components of the E-field in the $\phi = 0$ plane, for different numbers of turns of the helix antenna. (Turns are indicated on the plot.)

6. Transient Measurements for a 4-Turn Helix

Measurements of the transient radiated field from a 4-turn helical antenna when driven by the 500 MHz switched oscillator have also been made. To minimize the possibility of flashover near the source feed, we used some insulating plastic at the base of the helix, as indicated in Figure 34. The nylon insulating material was reduced to the minimum required to improve SWR of the antenna. The position of the lower loop of the helix relative to the ground plane was adjusted to optimize S_{11}.

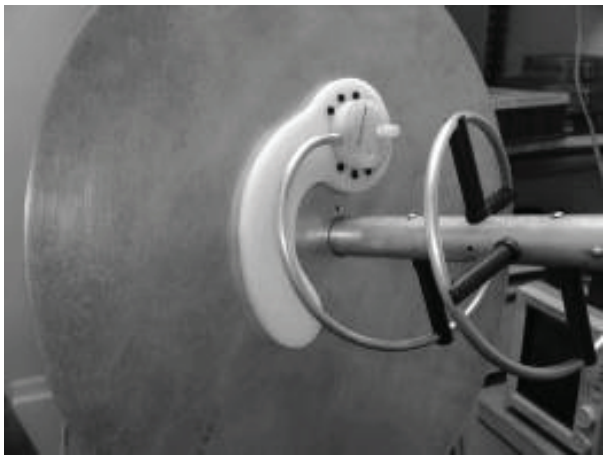

Figure 34. Switched oscillator/antenna interface and the measured S_{11}

The measured S_{11} and the input impedance as a function of frequency are shown in Figure 35. It is clear from the S_{11} measurements that the antenna has an acceptable bandwidth extending from 400 MHz to 600 MHz. The approximate impedance magnitude in the mesoband (400 MHz to 600 MHz) appears to be about 90 Ω.

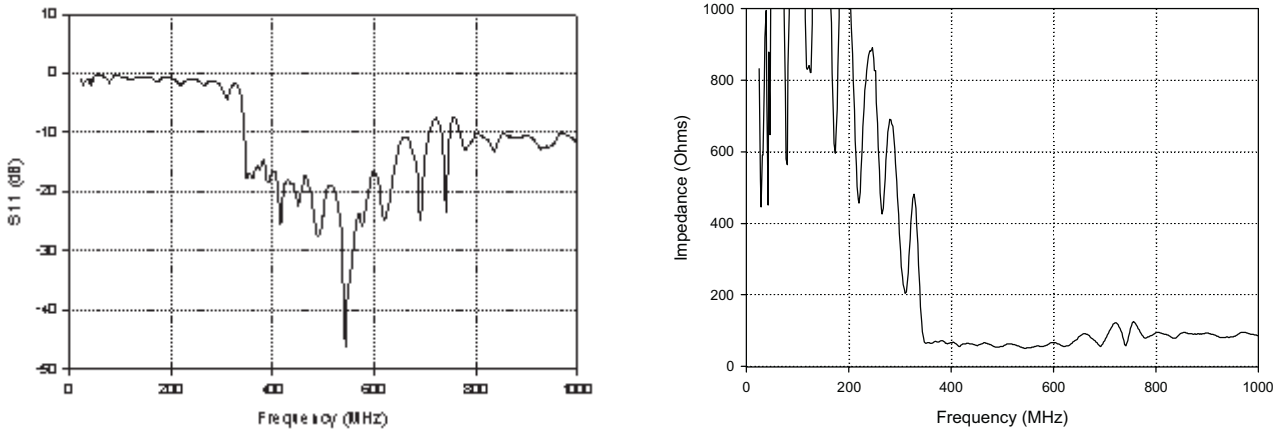

a. S_{11} b. $|Z_{in}|$

Figure 35. Measured S_{11} and input impedance magnitude for the 4-turn helix, shown as a function of frequency.

A reference sensor (shown in Figure 36) is mounted on the ground plane between the helix and the ground plane. This reference sensor measures the voltage applied to the helix to normalize the field data for shot variability. The reference sensor signal is also used to trigger the oscilloscope.

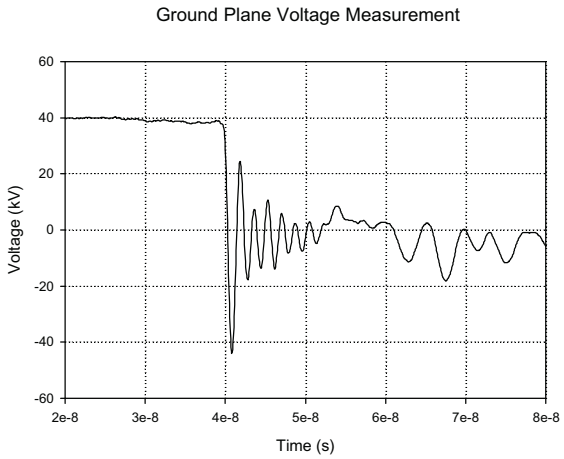

Figure 36. Reference sensor on the ground plane and the measured voltage.

Within the clear time of the reference sensor, the measurements show that we have a 500 MHz (a 2ns period) damped sinusoidal signal with an amplitude of about 40 kV and a Q in the range of 5 to 6 applied to the helical antenna.

B-field measurements for the 4-turn helix were made and are summarized by the following:

- The primary radiated B-field components were measured using a single Prodyn Technologies B-60 magnetic field sensor,
- An effective E-field was computed, under the assumption of the plane wave relationship E = 377 H is valid for each set of radiated components,
- The distance from the end of the helix to the test point was 1m and 2m,
- The available clear time for measurements is approximately 6 ns, and
- Measurements were made on and off bore site in 10 degree increments

The two components of the transient electric fields at distances of 1 and 2 meters are shown in Figure 37 and Figure 38 respectively.

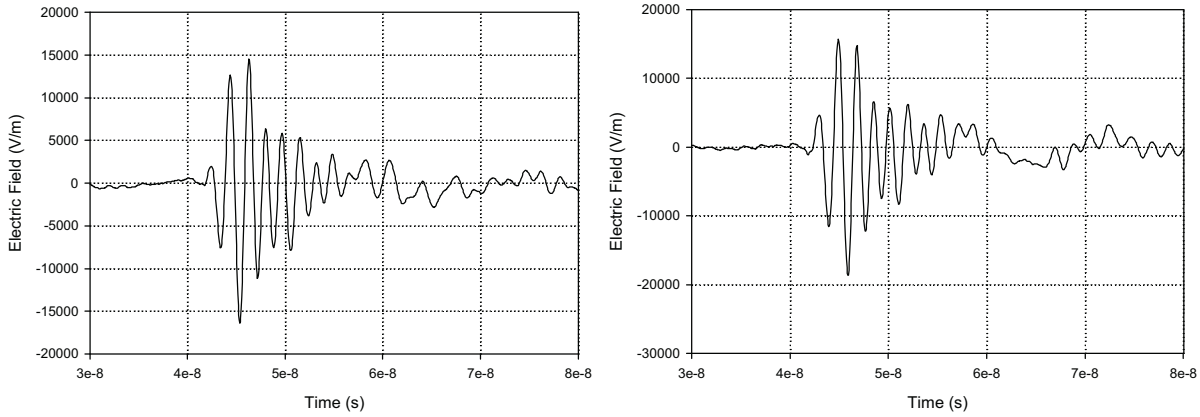

a. Vertical or phi component b. Horizontal or theta component

Figure 37. Two components of the measured electric field (circularly polarized) at a distance of 1m.

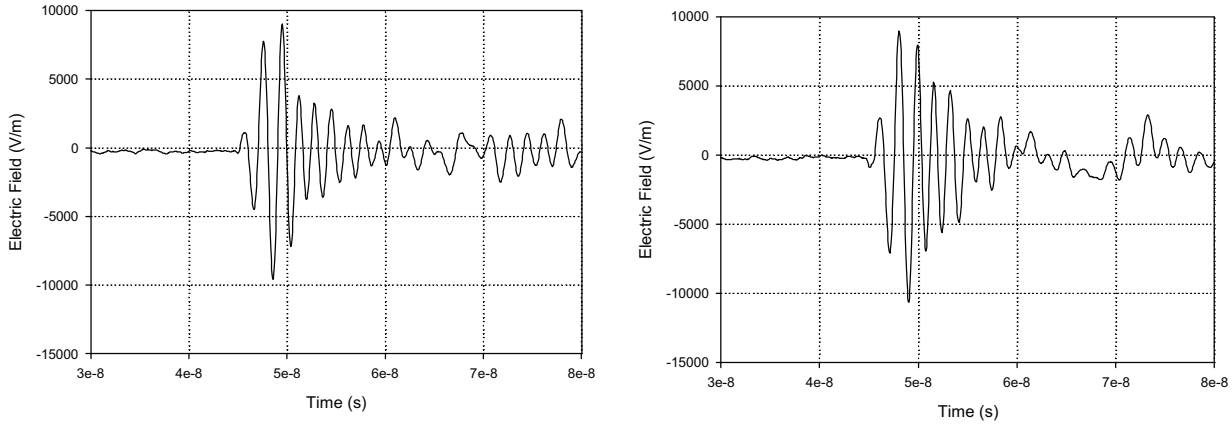

a. Vertical component b. Horizontal component

Figure 38. Two components of the measured electric field (circularly polarized) at a distance of 2m.

An overlay of the two components of the electric field at 1m and 2m distances are shown in Figure 39 and Figure 40, respectively. Figure 41 presents the measured total angular radiation patterns in both Cartesian and polar plots.

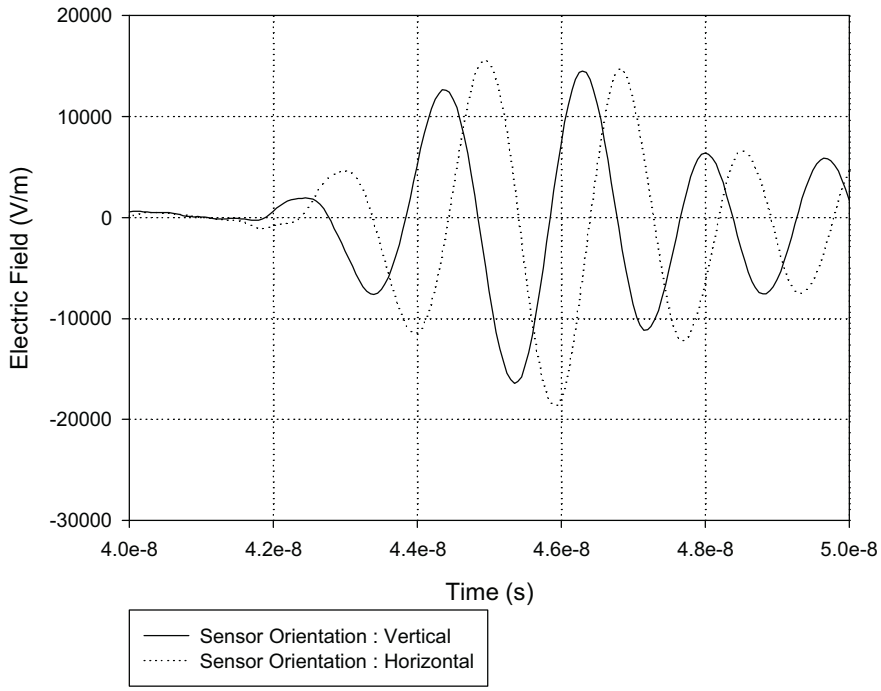

Figure 39. Overlay of the vertical and horizontal components of the measured transient electric field at 1m distance, demonstrating a nearly circular polarization.

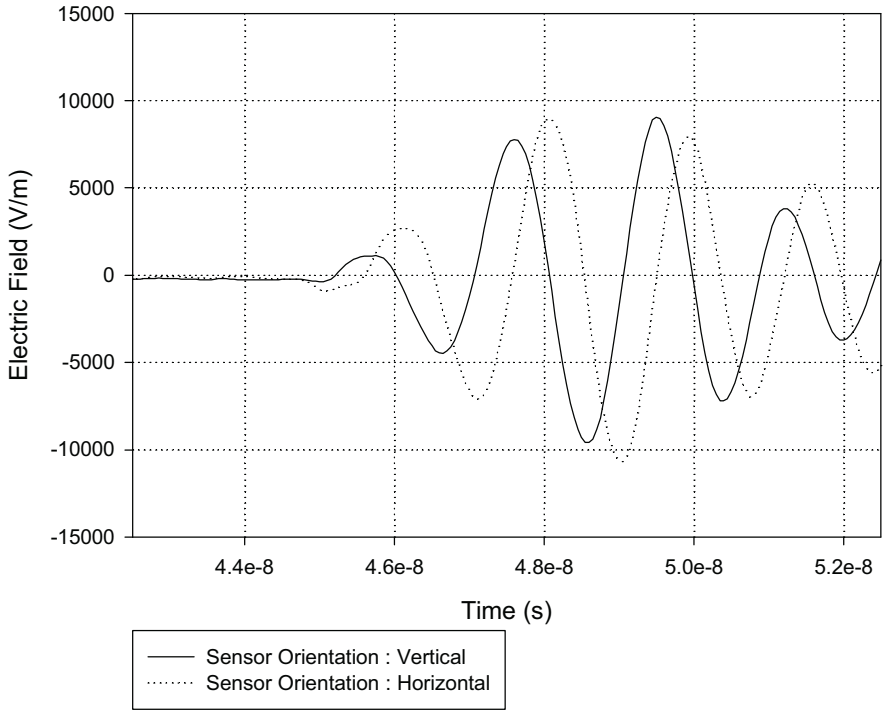

Figure 40. An overlay of the two components of the measured transient electric field at 2m distance demonstrating a nearly circular polarization.

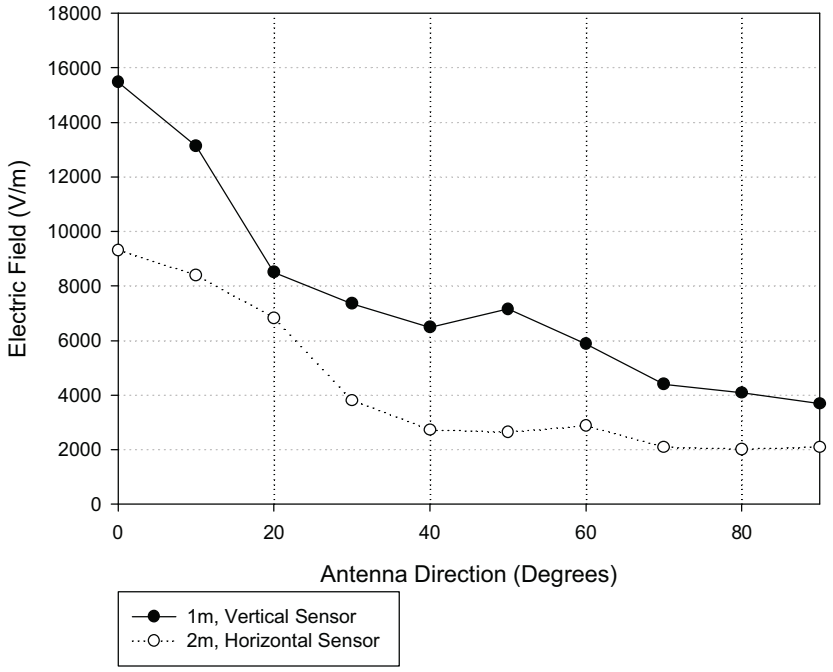

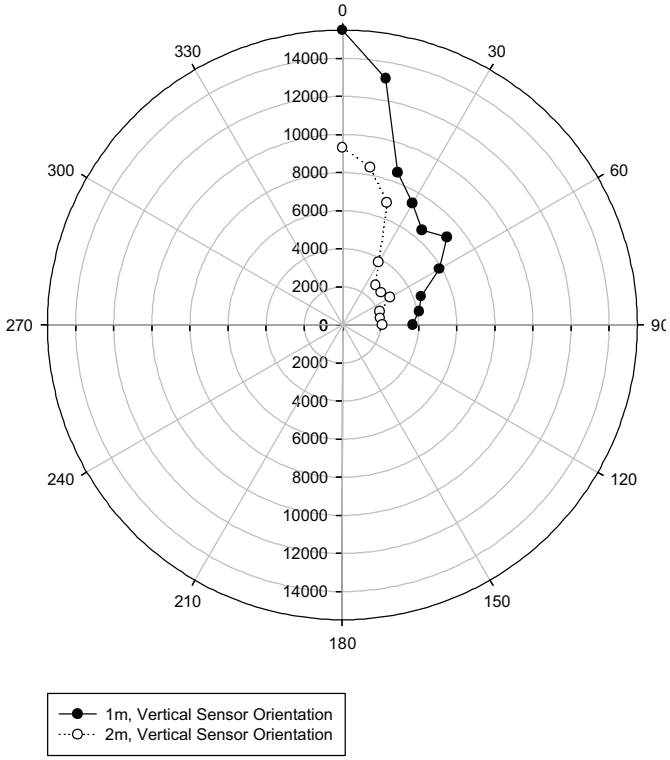

Figure 41. Measured radiation patterns of the 4-turn helical antenna.

The spectral content of the measured transient fields are also obtained, by performing FFTs of the transient data. They are shown in Figures 42 to 44.

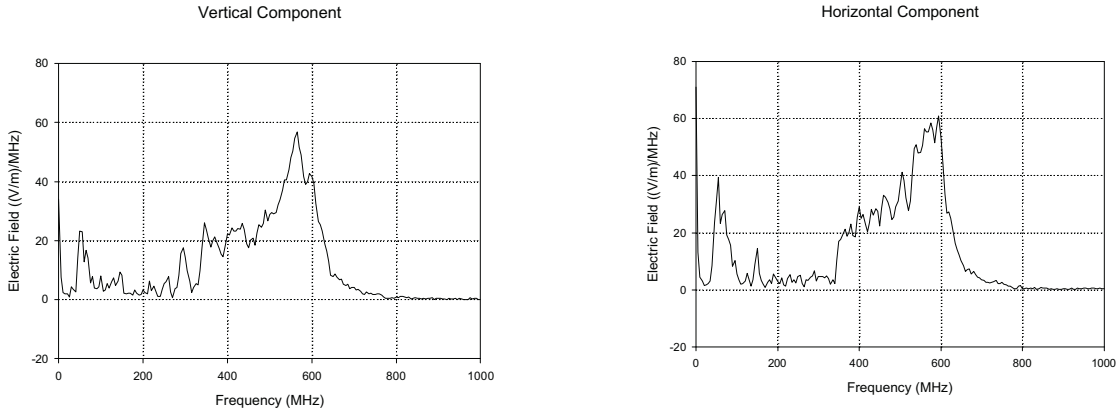

Figure 42. Spectra content of the boresight electric field (vertical or theta component) and horizontal or phi component at a distance of 1m

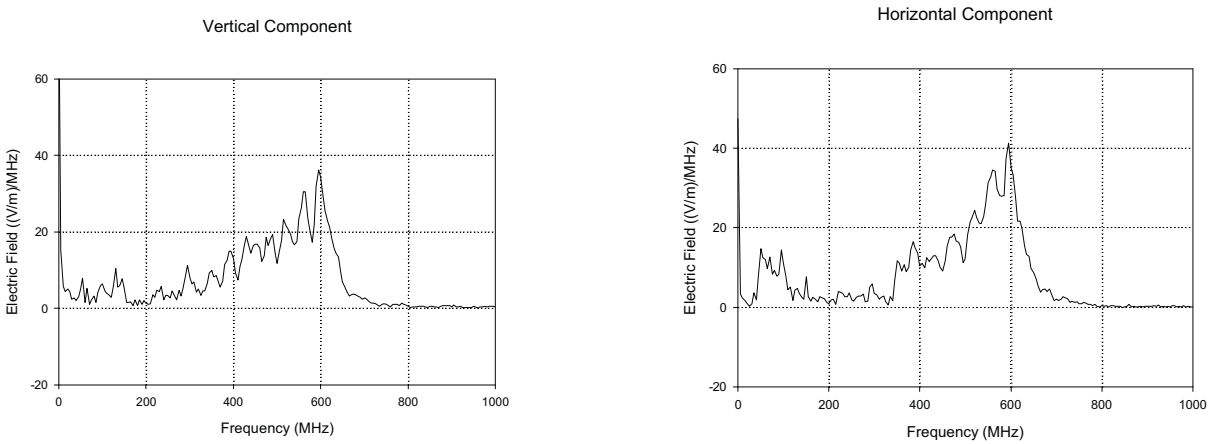

Figure 43. Spectra content of the boresight electric field (vertical or theta component) and horizontal or phi component at a distance of 2m

7. Comparing the Measurements with the Computations

The computations for the radiated - transient fields were done for a 10-turn helix and reported in Figure 30 for three different values of Q (1, 10 and 100) of the excitation waveform. For each of the two components, the peak electric fields at 1m distance (from Figure 30) are 20 kV/m, 50 kV/m and 70 kV/m for the three values of Q. The measured peak electric field of either component at a distance of 1m is about 15 kV/m (Figure 39). The higher values of computed fields can be attributed to the following:

1) The computations assume that about 50 kV of transient voltage peak is launched on to the antenna from charging the source to 30 kV. In reality, this could be a lot less depending on the actual impedance mismatch between the source and the antenna. The calculated impedance at 500 MHz is ~ 100 Ohms, whereas the measured impedance is half of that. Consequently, the launched voltage is only 35 kV and not the 50 kV assumed in the calculations. The input impedance of the antenna in the meso-band is a strong function of the feed point details, not all of which are considered in the computation (ex: effects of the oil dome and the insulting plastic at the base of the antenna introduced for voltage standoff etc.).

2) The computed fields are for 10 turn antenna and the measurements are for a 4-turn antenna, so the computed fields need to be adjusted down by about 30% (not quite linear, but sub-linear).

3) The computations were done for three values of Q (1, 10 and 100). Perhaps the value of Q = 10 is closest to being real value of Q out of the source.

The 50 kV/m peak field (one of two components) needs to be adjusted for: 1) the correct value of Q, 2) multiplied by 0.7 to adjust for the 4 turns in the measurement and 3) assumed 50 kV launch voltage. There are uncertainties in the Q, the impedance mismatch and we can only say the measurements agree with the computations qualitatively.

8. Summary

We have addressed the problem of designing, fabricating and testing switched oscillators at four different frequencies, 200MHz, 300MHz, 400MHz and 500 MHz. These oscillators are quarter wavelength long coaxial transmission lines with a nitrogen spark gap switch at one end. We have also fabricated two of these at 200MHz and 500 MHz with a charge voltage of 30 kV. These two oscillators are modeled using PSpice and their output into a 100 Ω load is estimated and tested by fabricating a 100 Ω transmission line. We have then proceeded to use a modified commercial helical antenna with a bandwidth of 400MHz to 600MHz and integrated the switched oscillator into this helical antenna. Measurements have been made of the S_{11}, voltage into the antenna and also transient fields at two distances. *Indeed, starting from electrical power from a 12V battery, electrical field strengths in excess of 10kV/m with damped sinusoidal waveforms at 500 MHz (for example) have been demonstrated.* In summary, 4 switched oscillators are designed, 2 have been fabricated and one of them has been integrated into a helical antenna to form a complete autonomous system. There are

uncertainties in the Q of the source in the measurement and the impedance mismatch between the source and the antenna. Consequently, we can only say the measurements agree with the computations qualitatively.

References:

1. C.E. Baum, "Switched Oscillators," *Circuit and Electromagnetic System Design Note 45*, 10 September 2000.

2. C. E. Baum, "Antennas for Switched Oscillators," *Sensor and Simulation Note 455*, 28 March 2001.

3. D. V. Giri, **High-Power Electromagnetic Radiators: Nonlethal Weapons and Other Applications**, published by Harvard University Press, 2004 , Section 5.5, pp 117-136.

4. J.W. Burger, C.E. Baum, W.D. Prather, R. Torres, D.V. Giri, M.D. Abdalla, M.C. Skipper, B.C. Cockreham, J. Demarest, K. Lee and D. McLemore, "*Modular Low Frequency High Power Microwave Generator***,**" presented at AMEREM 2002, Naval Academy, Annapolis, MD.

5. J. Lawrance, C.E. Baum, W.D. Prather, R.J. Torres, J. MacGillivray, M.D. Abdalla, M.C. Skipper and D.V. Giri**, "** *High –Power Mesoband Sources,***" ICEEA, Torino, September 2005.**

6. The WIPL-D computer code is described at http://www.wipl-d.com.